Wahyu Widhi Dyatmika

Towards the Application of Generalised Richardson Extrapolation in Spanwise Oscillating Wall Flow Control Analysis

SCHOOL OF AEROSPACE, TRANSPORT AND MANUFACTURING
Computational Fluid Dynamics

MSc
Academic Year: 2023 - 2024

Supervisor: Tamás Józsa
19th August 2024

SCHOOL OF AEROSPACE, TRANSPORT AND MANUFACTURING
Computational Fluid Dynamics

MSc

Academic Year: 2023 - 2024

Wahyu Widhi Dyatmika

Towards the Application of Generalised Richardson Extrapolation in Spanwise Oscillating Wall Flow Control Analysis

Supervisor: Tamás Józsa
19th August 2024

This thesis is submitted in partial fulfilment of the requirements for the degree of MSc

Academic Integrity Declaration

I declare that:

- the thesis submitted has been written by me alone.
- the thesis submitted has not been previously submitted to this university or any other.
- that all content, including primary and/or secondary data, is true to the best of my knowledge.
- that all quotations and references have been duly acknowledged according to the requirements of academic research.

I understand that to knowingly submit work in violation of the above statement will be considered by examiners as academic misconduct.

Abstract

Flow control is used to limit the adverse impact of a system on climate change. Several techniques have been tested and evaluated in terms of the net power savings achieved. One of the flow control methods, spanwise oscillating wall flow control has been observed to provide a positive net power saving (Marusic et al., 2021). Due to the impacts of large and small-scale turbulence, high-fidelity computational fluid dynamics simulations are typically used to analyse flow control performance. However, these simulation methods are computationally costly, particularly when high Reynolds numbers are used. This study demonstrates the effectiveness of Generalised Richardson Extrapolation as an approach for reducing simulation resources. This study discovered that the Richardson Extrapolation can forecast the ideal values in both uncontrolled and controlled channel flow instances. However, the extrapolation is limited to first-order statistics. When using Generalised Richardson Extrapolation to estimate second-order statistics, such as Reynolds stress tensor components, the result is massively overestimated. Additionally, the extrapolation outcomes are heavily influenced by coarse, medium, and fine resolution, necessitating rigorous control over the resolution of the sample models. Moreover, the results in this study demonstrate how Generalised Richardson Extrapolation functions in terms of predicting simulation results, as well as the algorithm's predicting performance. With this study, Generalised Richardson Extrapolation can be utilised in future DNS simulations to push the simulation limitations to flow regions that were not previously possible.

Acknowledgement

I would like to thank Dr. Tamás Józsa, my project supervisor, for his invaluable guidance in helping me develop my thesis project. His constant dedication and meticulous attention to detail have been crucial in completing this project. I am thankful that he gave me the chance to work on this project and beyond.

I am also grateful to the Indonesian Ministry of Finance for providing financial support in the form of LPDP Scholarship for my studies at Cranfield University. I am able to conveniently support myself overseas owing to the funding.

In addition, I would like to thank my parents, and my little brother for the constant guidance and affection; Esa Panganti Widoretno for all of her support and encouragement; all of the PPI Cranfield members for making this place feel like home; and my classmates, in particular Kilyan Ocampo Cardenas, Shivane Patel, and Ricardo Ortega del Angel, for their invaluable assistance with the course's endless assignments.

Contents

List of Figures

List of Tables

List of Symbols and Abbreviations

Abbreviations

ASCR	Asymptotic Grid Convergence Ratio
CFD	Computational Fluid Dynamics
CF	Channel Flow
CR	Coarse Resolution
CU	Computational Unit
DNS	Direct Numerical Simulation
FR	Fine Resolution
FstR	Finest Resolution
GCI	Grid Convergence Index
GREP	Generalised Richardson Extrapolation
HPC	High Performance Computing
ISA	Inner-Scale Actuation
LES	Large-Eddy Simulation
MR	Medium Resolution
NC	No Control
NPS	Net Power Saving
NR	Normalised Resolution
OSA	Outer-Scale Actuation
Osc	Spanwise oscillating wall flow control applied
PF	Pipe Flow
RANS	Reynolds Averaged Navier Stokes
RMS	Root Mean Square

Variables (Latin Letters)

A	Amplitude
a, b	Compact scheme variable
$\mathcal{A}$	Convection-diffusion operator
E	Energy
e	Vector component
f	Concerned values
F	Transport variable
F_s	Safety factor
g	Gravitational vector
h	Height
k	Phase difference
L	Domain length

L_o	Integral length scale
N	Number of grids
> N_{nodes}	Number of nodes
N_{proc}	Number of processors
$N_{t,spinup}$	Number of iteration required for sampling to start
$N_{t,spinup}$	Number of iteration for spinup
$N_{t,warmup}$	Number of iteration for warmup
n	Variable for showing time step
p	Pressure
$\mathcal{P}$	Order of convergence
Re	Reynolds number
R	Radius
r	Grid refinement ratio
s	Computational coordinate
t	Time
$t_{parallel}$	Time required to do parallel simulations
t_{serial}	Time required to do serial simulations
t_{tot}	Total time
$t_{wallclock}$	Wallclock time
u	Velocity vector
$u.\ v, w$	Streamwise, wall-normal, and spanwise velocity, respectively
x, y, z	Streamwise, wall-normal and spanwise direction, respectively

Variables (Greek Letters)

α	Compact scheme variable
α_k	Runge-Kutta coefficients for time advancements
$\alpha_h, \beta_h, \gamma_h, \delta_h$	Stretching coefficient
δ	Characteristic length
η	Kolmogorov length scale
θ_k	Runge-Kutta coefficient for time advancements
κ	Wave number
λ	Minimal flow length
ν	Kinematic viscosity
μ	Dynamic viscosity
ρ	Density
Φ	Scalar quantities
τ_w	Wall shear stress
ϕ	Transported quantity
Ω	Wave frequency

Subscripts and Superscripts

$\hat{}$	Intermediate values
$+$	Wall-normal value
τ	Viscous quantities
b	Bulk quantities
e	Equivalent values

1 Introduction

In the subject of fluid dynamics, flow control can massively influence the performance of the flow around or inside an object. Designing a flow control method requires an intricate understanding of flow behaviours such as dynamics and turbulence. Designing a proper flow control can be essential for maximising the efficiency of the system.

1.1 Motivation

Climate change has been a driving factor for engineering design in the modern world [1]. The changes in climate patterns have proven to be detrimental to humans and other living beings. One of the causes of climate change is the emission of energy generation processes, such as carbon dioxide [2]. However, the need to create more energy is indispensable as the human population grows continuously, with energy requirements predicted to reach more than triple the global energy requirement today [3]. This requires engineers to create a high-performance solution with a consideration of efficiency in its operations. In the aerospace sector, this approach is also used as the sector creates 2% of the total global emission, which is the largest among other means of transportation [4]. Generally, in the aerospace sector, a high-efficiency value can be reached by minimising drag, which is generated from the viscous drag, as shown in Figure 1. The viscous drag can be practically reduced in a controlled manner using flow control strategies, offering a solution for a sustainable aerospace future [5].

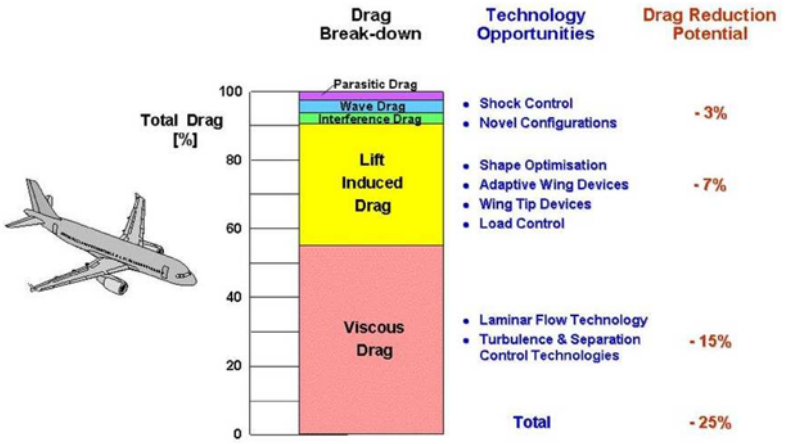

Figure 1: Drag and Reduction Potential in a General Aircraft [5]

Fluid flow control has been a major topic in fluid dynamics. Fluid flow control strategies have been implemented in various areas, such as aerospace, wind energy sector, industrial process designs, and water management [6]. The development of flow control methods was born from the understanding of the presence of turbulence in a fluid flow. Turbulence

in a moving flow can generally be denoted by the chaotic behaviour of the fluid [7], typically in the form of eddies or vortices. The interaction of the flow with itself, along with the solid object nearby can produce drag, which reduces the flow velocity and its ability to transport its properties [8]. In most systems, the drag can be detrimental as it can reduce the efficiency of the system. Because of that, flow control strategies are introduced to force the fluid to move in a regulated behaviour to decrease the drag produced in the system.

Currently, multiple strategies and approaches towards an efficient flow control system are studied. One of the recent studies [9] suggests that an active flow control strategy in the form of spanwise wall oscillations can generate a positive net power saving value for high Reynolds number regimes. With the finding, a pathway for an industrial-wide application of oscillating wall flow control can be opened and hence further studies are needed.

In order to further expand the spanwise wall oscillation flow control strategy, understanding the turbulence in the flow is of utmost importance, especially in the near-wall region. Turbulence is the chaotic nature of a fluid flow, caused by "a complex interplay of multiple flow patterns occurring simultaneously, making it difficult to model and predict accurately" [10]. Therefore, intricate physics modelling is generally required to completely simulate the turbulence in the flow, which is growingly expensive in terms of computational cost as the Reynolds number increases [11]. In this paper, direct numerical simulation (DNS) is introduced as a solution for high-fidelity simulation, incorporating generalised Richardson extrapolation to make the analysis time-efficient. This paper will mainly utilise the ARCHER2 HPC environment for generating the data to create a more efficient simulation.

1.2 Literature Review

1.2.1 Physics of Wall Bounded Flow Turbulence

Turbulence can be defined as the swirling motion that happens randomly in the fluid flow [12]. Due to its randomness, turbulence phenomena can sometimes be too complicated and difficult to comprehend [13]. Therefore, most turbulence studies are focused on understanding the coherent structures, which are the regions with recognisable concentrated vorticity [14]. As seen in Figure 2, there are common structures in the flow region near the wall that are identifiable. The most prominent structure is the hairpin vortex, which is indicated by a rising arch head with two streamwise-oriented legs [15].

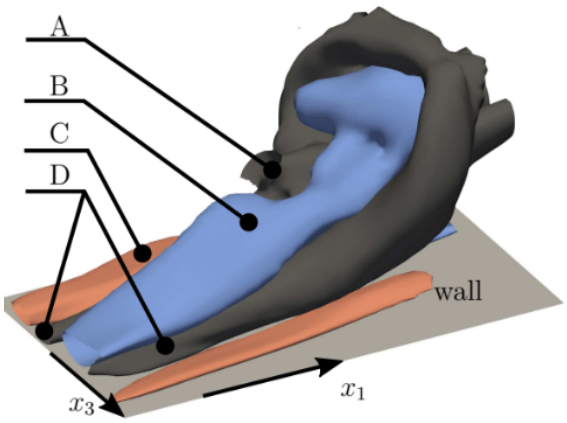

Figure 2: Near Wall Coherent Structures: A) Hairpin Vortex ; B) Low momentum region; C) high momentum region; D) counter-rotating quasi-streamwise vortices [16]

Several studies, such as the studies made by Wang [15] and Alfonsi [17] explained how the hairpin vortices are generated. First, the legs of the hairpin vortices, which consist of two quasi-streamline, counter-rotating vortices interacted with each other. These vortices rise to the area with lower shear magnitudes, which decreases the vorticity magnitude. With the opposing rotational direction, the coalescence of two vortical structures occurs and the hairpin vortices are generated. Inside the vortex, a low momentum region is generated. Conversely, the high momentum region is generated outside the two counter-rotating vortices.

Other than the physical structures, spectral analysis is also commonly conducted to understand the turbulence phenomena. Generally, spectral analysis involves analysing the turbulence through the wave energy distribution in the structures [18]. In order to visualise the energy distribution, the Kolmogorov spectrum is used, as shown in Figure 3.

Based on Brennen [19], there are 3 main regions in the spectrum. The first is the integral region, commonly known as the energy-containing range. This characterises the overall size of the largest eddies, which contain the energy in the flow. These large-scale structures are responsible for transferring energy from the external forces to the smaller structures in the turbulent flow. The energy then cascades to the smaller scales through the inertial region. The energy spectrum in this region follows a power law distribution:

$$E(k) \propto k^{\frac{5}{3}} \tag{1}$$

Where k is the wave number. Afterwards, the energy cascades to the smallest scales, which are in the Kolmogorov scales. In this scale, the viscosity dominates and the kinetic energy is transferred to heat energy.

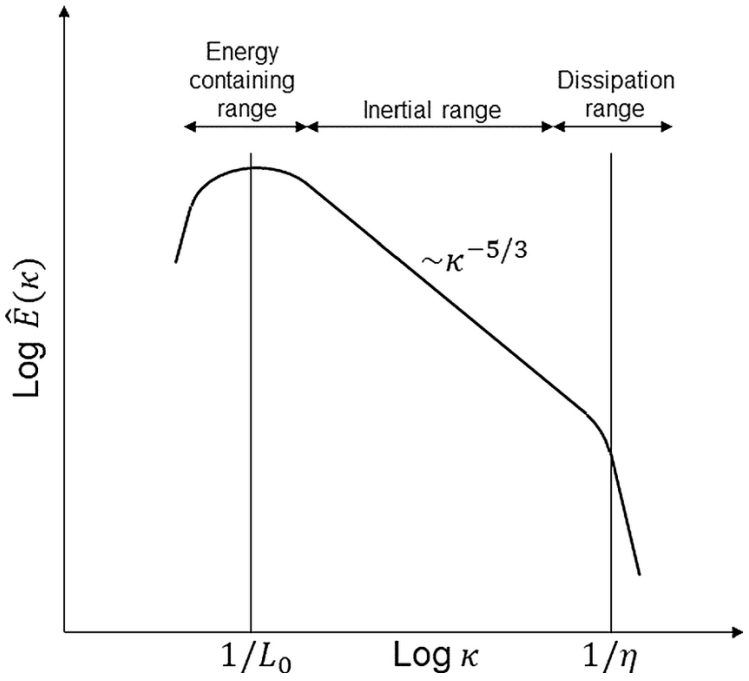

Figure 3: Typical Energy Spectrum in a Flow [20]

1.2.2 Spanwise Oscillating Wall Flow Control

Flow control can be defined as the method of altering the flow to a desired state or path [21]. Typically, there are two types of flow control methods, as stated by Ricco [22]. The first method is passive flow control, which requires no actuation or movement in the system, thus no external energy is required to control the fluid flow. The second method is the active flow control. Contrary to its passive counterpart, active flow control requires energy to actuate a motion in a flow.

Due to the certain energy consumption, most of the studies regarding active flow control are circulated around the strategy to create a motion that has a positive net power saving. The same trend has been observed for the spanwise oscillating wall method, which requires actuation to create an oscillation in the near wall region. The concepts and methods are documented in Table 1.

Table 1: Experimental and Computational Studies of Spanwise Oscillating Wall Flow Control

References	Geometry	Methodology	Reynolds Number	$\mathbf{NPS}_{max}$ (%)
Marusic et al. (2021) [9]	CF	Experimental: Hot-wire anemometry Computational: LES (dynamic Smagorinsky)	Re_τ = 6000 Re_τ = 12800	∼7 ∼2
Gatti and Quadrio (2016) [23]	CF	Computational: DNS	Re_τ = 200 Re_τ = 1000	5.3 ± 0.24 3.9 ± 0.31
Quadrio et al. [24]	CF	Computational: DNS	Re = 4760	5
Auteri et al. (2010) [25]	PF	Experimental, with DNS comparison from [24]	Re = 4760	17
Viotti et al. (2009) [26]	CF	Computational: DNS	Re_τ = 200	23
Chandran et al. (2023) [27]	CF	Experimental: Drag Balance and Hot Wire Anemometry	$4500 \leq Re_\tau \leq 150000$	ISA: -40 OSA: 5-10
Deshpande et al. (2024) [28]	CF	Computational: DNS	$Re_\tau \approx 300$	Not reported
Nguyen et al. (2021) [29]	CF (with square bar)	Computational: DNS	Re_τ = 218	0.8
Ricco et al. (2012) [30]	CF (rough wall)	Computational: DNS	Re_τ = 200	Not reported

The key trend from the results is the NPS value is dependent on various factors. It is apparent from the studies that the NPS value of the flow control decreases as the Reynolds number increases [23] [24]. Other than that, the net power saving also relies on the wave function applied. From the studies, it can be seen that the net power saving is positive when the wave function of the oscillating wall matches the large-scale eddies inside the flow [9][27].

Based on the table, a simple channel flow is the most common base case to test the effectiveness of flow control. This is due to the simplicity of the flow modelling as the case only has two wall surfaces, generally placed on the top and the bottom of the domain. The domain surfaces on the side are assumed to be free surfaces [31]. For the boundary condition assignment, the effect of the wall in the flow will be easier to analyse without having to take into account the wall perpendicular to the wall of interest.

1.2.3 Turbulence Modelling

Solving turbulence is required in order to create a good model of a fluid flow. This is because turbulence is highly related to the transport of mass, energy, and other values in the flow [32]. However, variety in the temporal and spatial scale of turbulence oftentimes requires high computational power [33]. To alleviate the excessive computational power, turbulence modelling is often used, generally in the form of Reynolds Averaged Navier Stokes (RANS) [34]. However, due to the nature of the modelling, some simplifications lead to information loss, especially regarding the energy cascade to the small scales [35]. Another approach that can be done is using the Large Eddy Simulation (LES). LES method solves large eddies directly but uses modelling to solve the small eddies [36]. This way, high accuracy can be obtained for the large structures, while maintaining low computational expenses. However, similar to RANS modelling, inaccuracy can occur in small-scale turbulence [37].

In cases where the effect of small-scale turbulence is heavily considered, turbulence modelling is fully disregarded. This means that the Navier-Stokes equations are directly solved [38]. This method of solving the fluid flow is termed Direct Numerical Simulation (DNS). Ideally, DNS should be performed with spatial resolution at least as large as the Kolmogorov scale, which is the smallest eddies that can be produced by the flow [39]. However, the fine grid resolution will make the analysis prohibitively expensive. Therefore, lower resolution is usually preferred to DNS methods.

1.2.4 Grid Convergence and Generalised Richardson Extrapolation

A certain confidence in the result must be the base of a computational simulation. Confidence is needed so the result can be applicable and have a good degree of reflecting

the physical phenomena of the problem. In CFD, confidence is built by proving the consistency of the result using a grid convergence study (GCS), which was introduced by Roache [40]. Grid convergence study involves a minimum of 3 different simulation models with resolution variation, generally named as coarse, medium, and fine model [41]. The resolution of the models is variated using the following relation

$$N = 2^n m + 1 \tag{2}$$

The domain settings may change the value of the results. The finer the settings are, the higher the quality of the results. However, finer results require high computational resources which limits the resolution of the model. To counter the problem. the Richardson extrapolation is usually used. Richardson extrapolation can be defined as the approximation of the ideal value of convergent value using [40]:

$$f_{h=0} \simeq \frac{4}{3} f_1 - \frac{1}{3} f_2 \tag{3}$$

However, most of the applications of Richardson extrapolation are limited to spatial convergence. The novel method of Richardson extrapolation includes temporal and domain size to determine the best resolution of a computational case.

1.2.5 Xcompact3D

The research mainly uses Xcompact3D to solve the fluid flow. Xcompact3D is a FORTRAN 90-based open-source software purposed to simulate incompressible fluid flows [42]. The software uses high-order compact schemes [43], which utilise shortened versions of high-order schemes. This way, the analysis will still satisfy the need for high resolution of high-order schemes, while maintaining the simplicity of low-order schemes [44], making the compact schemes a powerful and efficient tool to solve turbulence.

With the higher-order schemes, the simulation can run high-fidelity schemes to solve the viscous terms in the Navier-Stokes equation. The two models that are available to use in Xcompact3D are Large Eddy Simulation (LES) and Direct Numerical Simulation (DNS) [43]. As the section 1.2.3 suggests, both methods are preferable when it comes to analysing turbulence in detail.

1.2.6 High Performance Computing

This study massively used HPC environments. Using HPC environments, the simulation can be accelerated to an extent with the increase in number of cores. Commonly, the acceleration is measured by the scalability parameter, which is the measure of the simulation

time affected by the problem size and number of workers or cores [45]. The scalability result is case-specific, thus every algorithm and the different case will result a different scalability results.

Generally, there are two different methods of measuring scalability [46]. The first is the strong scaling, which expresses the solution time variation with the number of processors for a fixed total problem size. The strong scaling speedup is generally calculated using Amdahl law, which is expressed as the following [47]:

$$speedup = \frac{1}{\left(\frac{t_{serial}+t_{parallel}}{N_{proc}}\right)} \tag{4}$$

The second method is the weak scaling. The scaling method expressed the solution time variation relating to the number of processors for a fixed problem size per processor. The weak scaling method utilises the Gustafson law [48], shown below.

$$scaledspeedup = t_{serial} + t_{parallel} \times N_{proc} \tag{5}$$

Another thing to consider when considering HPC services for simulation is the resources required. In ARCHER2, the resources allocated for the simulated are calculated in CU units, which is calculated as [49]:

$$CU = N_{nodes} \times t_{wallclock} \times N_{jobs} \tag{6}$$

The cost required for the CU resources can also be calculated. The cost is calculated in pounds.

$$Cost_{CU} = CU \times 0.20 \tag{7}$$

1.2.7 Knowledge Gap

Current spanwise oscillating wall flow control research lacks a thorough analysis of high Reynolds numbers. To conduct flow control studies using CFD, researchers must analyse turbulence in great depth, usually using LES or DNS analysis. This leads to high computational expenses. The expensiveness in the analysis is also exacerbated by the common practice of utilising a very large domain with a fine resolution, which makes the analysis in a high Reynolds number particularly impossible. In this study, Generalised Richardson Extrapolation is introduced by varying the spatial and temporal resolution alongside sample and domain size to decrease the computational requirement of the flow control analysis.

1.3 Aim and Objectives

The aim of this study is to analyse the effectivity of Generalised Richardson Extrapolation in the numerical analysis of spanwise oscillating wall flow control.

With this aim, the objectives can be set as the steps to achieve the aim set. The objectives are set as follows:

- Introduce Xcompact3D in the HPC environment, particularly CRESCENT2 and ARCHER2 environment
- Run a laminar flow around a cylinder case as the test case in Xcompact3D
- Generate turbulent channel flow cases as the main test cases for the study
- Generate Generalised Richardson Extrapolation analysis by changing the spatial and temporal resolution
- Conduct flow simulations of the channel flow with and without spanwise oscillating wall flow control using DNS

1.4 Synopsis

The thesis is arranged to be in a form as follows. Section 2 provides the theoretical background and the methodology for the thesis. The governing equations, along with the supporting equations used in the numerical simulations are thoroughly explained. Moreover, the computational procedures, including geometry and mesh generations, simulation settings and post-processing methods are introduced in this section.

Results obtained from the analysis are displayed in Section 3. The discussion is then served as the rationale for the result. Several figures and tables are displayed as a summary of the result and an aid for understanding the phenomena behind the flow condition. Section 4 presents the conclusions of the current study and recommendations for future studies.

2 Methodology

2.1 Flow Problem of Interest

2.1.1 Laminar Flow Around a Cylinder

In this case, a cylinder is subjected to a flow that creates an oscillating wake vortices, which is commonly known as the vortex shedding phenomenon. The parameters of the cylinder are set as shown in the input example. The parameters of the cylinder are set as given by the Xcompact3D input example, shown in Table 2.

Table 2: Cylinder Wake Case Parameters

Re	x_{cyl}	y_{cyl}	R_{cyl}	u_b	ρ	ν
300	5	6	0.5	1	1	0.0033

It is important to note that the cylinder wake case is solely used to test the quality of the Xcompact3D case. Therefore, the cylinder case will not be analysed as in-depth as the channel flow cases.

2.1.2 Channel Flow

To understand the influence of oscillating wall flow control on a turbulent flow, a case must first be formulated. Generally, the case used is a canonical flow problem, in which the information and data are abundantly accessible and can easily compared to one another. With comparable data, the turbulence phenomena could be thoroughly explored. This paper uses a simple double periodic channel flow case to investigate the oscillating wall flow control problem. Double periodic channel flow cases utilise periodic boundary conditions to two sets of planes: spanwise and streamwise. The wall-normal plane boundary condition is set to the wall boundary condition, in which the flow would be affected.

When simulating a double periodic channel flow problem, the first step is to establish the required channel flow domain size. The domain size must be carefully set to limit computing costs while yet capturing all of the relevant turbulence features. Figure 4 illustrates the minimal flow unit, which is the smallest size of double periodic channel flows [50].

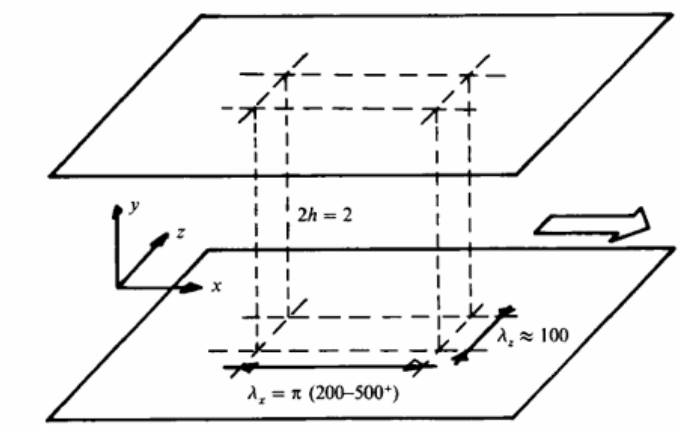

Figure 4: Minimal Flow Unit of a Double Periodic Channel Flow [50]

The length of the minimal flow unit is defined in a wall flow unit, denoted by the (+) sign. The (+) sign is a normalisation of quantities using the viscous length scale, formulated as:

$$\delta_\nu = \frac{\nu}{u_\tau} \tag{8}$$

The friction velocity u_τ is a function of wall friction, defined as [51]:

$$u_\tau = \sqrt{\frac{\tau_w}{\rho}} \tag{9}$$

Wall shear stress τ_w is related to the Reynolds number and the velocity gradient to the normal direction stated as [52]:

$$\tau_w = \frac{\partial u}{\partial y} Re \tag{10}$$

Re is the dimensionless number which displays the ratio between the inertial and viscous forces, expressed as [53]:

$$Re = \frac{v\delta}{\nu} \tag{11}$$

For studies in turbulence, friction Reynolds numbers are more commonly used due to their relevance to near-wall turbulence. The equation of the friction Reynolds number is displayed below [51].

$$Re_\tau = \frac{u_\tau \delta}{\nu} \approx 0.09(2Re)^{0.88} \tag{12}$$

For the base case, the Reynolds number is defined as $Re_\tau = 180$. The quantity is chosen due to the availability of DNS channel flow data [54] and the data from Xcompact3D [42]. The fluid properties data is shown in the Table 3 below.

Table 3: Fluid Properties

Re_τ	Re	u_b	ρ	ν
180	2819.294	1	1	0.00035

2.2 Theoretical Background

2.2.1 Governing Equations of Incompressible Fluid Flow

In a low Reynolds number scenario, as specified in Section 2.1, the fluid becomes incompressible, transforming both governing equations of fluid flow [55]. For the continuity equation, the expression reduces to:

$$\nabla \mathbf{u} = 0 \tag{13}$$

The bold variables denote a field. For the context of $\mathbf{u}$, which is the velocity field, it can be expanded into:

$$\mathbf{u} = u\mathbf{e_x} + v\mathbf{e_y} + w\mathbf{e_z} \tag{14}$$

In contrast, the momentum equation changes when the compressibility element is removed. Furthermore, because there is no height change in the channel flow, the gravity term is omitted. Furthermore, the momentum equation may be changed by normalising each component to density, which remains constant in incompressible flow. The momentum equation for incompressible flow can be expressed as:

$$\underbrace{\frac{\partial \mathbf{u}}{\partial t}}_{\text{I.}} + \underbrace{(\mathbf{u} \cdot \nabla)\mathbf{u}}_{\text{II.}} = \underbrace{-\frac{1}{\rho}\nabla p}_{\text{III.}} + \underbrace{\nu \nabla^2 \mathbf{u}}_{\text{IV.}} \tag{15}$$

There are four members in an incompressible Navier-Stokes equation. The term I is the unsteady term, showing the change of the fluid velocity over time. The term II is the convective term, showing the transport of properties in the flow. The third term is the pressure gradient, showing the change of pressure in the fluid. Lastly, term IV, determines how the viscous diffusion and dissipation affect the flow.

2.2.2 Fractional Step Method

In incompressible flows, the density remains constant while the pressure varies. As a result, the equation of state is not applicable [55]. Therefore, the pressure and velocity equation must be solved together in a coupled equation. Xcompact3D utilises the Fractional Step Method [56]. The Fractional Step Method involves four stages to link the pressure and

velocity variables [57]. The first phase uses the intermediate velocity field, represented as [58]:

$$\frac{\hat{\mathbf{u}}^k - \mathbf{u}^{k-1}}{\Delta t} = \gamma_k \mathcal{A}(\mathbf{u}^{k-1}) + \theta_k \mathcal{A}(\mathbf{u}^{k-2}) - \alpha_k \nabla p^{k-1} \tag{16}$$

Where $\mathcal{A}$ is the convection-diffusion operator, which includes both terms II and IV of the Navier-Stokes equations [16]. It is also worth noting that the intermediate velocity field does not satisfy the continuity equation due to its divergence-free characteristics.

Then, the second step is to solve the predicted scalar field, using the following relation:

$$\nabla^2 \phi^k = \frac{1}{\alpha_k \Delta t} \nabla \hat{\mathbf{u}}^k \tag{17}$$

This step is based on the pressure-Poisson equation, which makes this step computationally demanding [16]. Therefore, the 3D FFT scheme is used to solve the scalar field equation [59].

The third step is to update the velocity using the known scalar field and intermediate velocity field.

$$\mathbf{u}^k = \hat{\mathbf{u}}^k - \alpha_k \Delta t \nabla \phi^k \tag{18}$$

Finally, the pressure field is updated using the relation with the scalar field:

$$p^k = p^{k-1} + \phi^k \tag{19}$$

2.2.3 Spatial Discretisation

Solving the Navier-Stokes equation numerically requires spatial discretisation, which involves transferring the properties of the flow from one member to another [60]. Xcompact3D uses various types of compact finite difference schemes [44], due to its ability to solve the derived values of a defined point and the neighbouring members simultaneously. This study uses the 6th-order centred Hermitian compact scheme, which solved the first derivation of the values as: [61]:

$$\alpha \mathbf{u}'_{i-1} + \mathbf{u}'_i + \alpha \mathbf{u}'_{i+1} = a \frac{\mathbf{u}_{i+1} - \mathbf{u}_{i-1}}{2\Delta x} + b \frac{\mathbf{u}_{i+2} - \mathbf{u}_{i-2}}{4\Delta x} \tag{20}$$

For the variables, it is set into $\alpha = 1/3$, $a = 14/9$, and $b = 1/9$ to ensure the scheme can represent a wide range of turbulence scales [44]. The second derivative also uses the 6th-order central scheme, expressed as:

$$\alpha \mathbf{u}''_j + \mathbf{u}''_{j+1} + \alpha \mathbf{u}''_{j+1} = a\frac{\mathbf{u}_{i+1} - 2\mathbf{u}_i + \mathbf{u}_{i-1}}{\Delta x^2} + b\frac{\mathbf{u}_{i+2} - 2\mathbf{u}_i + \mathbf{u}_{i-2}}{4\Delta x^2} + c\frac{\mathbf{u}_{i+3} - 2\mathbf{u}_i + \mathbf{u}_{i-3}}{9\Delta x^2} \tag{21}$$

To ensure the same range as the first derivative, the variables α are set to 2/11, a is set to 12/11, b is set to 3/11, and c is set to 0. Using these equations and the said variables' value, the scheme can calculate the results with a 4 or 5 times lower number of mesh nodes compared to 2nd-order schemes while only increasing 2 times its computational expenses [56].

2.2.4 Temporal Discretisation

Other than spatial discretisation, temporal discretisation must also be applied to calculation so the numerical simulation can be progressed to the next time step. For nearly all of the time discretisation, the third-order Adam-Bashforth equation is used. The third-order Adam-Bashforth scheme is an explicit scheme that uses one equation to progress the time step of the calculation [62], displayed as:

$$\phi^{n+1} - \phi^n = \frac{\Delta t}{12}[23F^n - 16F^{n+1} + 5F^{n-2}] \tag{22}$$

Where

$$F^n = \mathbf{u}^n\phi^n$$
$$F^{n-1} = \mathbf{u}^{n-1}\phi^{n-1}$$
$$F^{n-2} = \mathbf{u}^{n-2}\phi^{n-2}$$

For the diffusion term in the wall-normal direction, the implicit Crank-Nicolson equation is also used for the time discretisation. The temporal discretisation for the y-diffusion term can be expressed as:

$$\left(\nu\frac{\partial^2 v}{\partial y^2}\right)^{n+\frac{1}{2}} = \frac{1}{2}\left(\nu\frac{\partial^2 v^{n+1}}{\partial y^2} + \nu\frac{\partial^2 v^n}{\partial y^2}\right) \tag{23}$$

2.3 Computational Procedures

2.3.1 Xcompact3D Setup

Xcompact3D, as any other FORTRAN F90-based code, must be downloaded and compiled before being able to be used as an analysis software. The code is downloaded through its official Github repository, using:

```
git clone https://github.com/xcompact3d/Incompact3d
```

After that, the code is compiled using the following commands on UNIX, assuming 8 threads are available for compiling the code:

```
cd Incompact3d
export FC=mpif90
cmake -S . -B build
cd build
cmake --build . -j 8
```

Then by going to the *input.i3d* file in each example code, the boundary conditions, as well as domain size, number of mesh, and initial condition can be changed.

2.3.2 Grid Generation

For the entirety of the study, the cartesian structured grid is used. The entire model is discretised into a system of hexahedral-shaped elements with eight nodes connecting to each other [63]. In a simple canonical flow as this study, the structured hexahedral grid is favoured due to the efficiency of the shape in terms of filling the spaces, as well as the ability to minimise diffusion when transferring the properties from an element to another [64]. Additionally, the simple connectivity of the elements makes the grid model simple to program [65].

To capture the near-wall turbulence, the size of the grid near the wall must be decreased. However, just uniformly decreasing the size of the grid may cause an unnecessary computational expense as the flow on the centre of the channel flow does not have substantial gradient or turbulence structures. To compensate for the problem, a stretching algorithm is introduced in the Xcompact3D program [44], developed from [66] and [67]. First, the domain must be expressed in physical coordinate y and computational coordinate s.

$$y = h(s), 0 \leq s \leq 1, 0 \leq y \leq L_y \tag{24}$$

The y-height of each member can be defined as

$$h = \frac{L_y\sqrt{\beta_h}}{\gamma_h\sqrt{\alpha_h}\sqrt{\alpha_h\beta_h}+1}\left\{\tan^{-1}\left(\frac{\sqrt{\alpha_h\beta_h}+1\tan(\pi(\gamma_h s+\delta_h))}{\sqrt{\alpha_h}\sqrt{\beta_h}}\right)\right.$$
$$\left.+\pi\left[H\left(s-\frac{1-2\delta_h}{2\gamma_h}\right)+H\left(s-\frac{3-2\delta_h}{2\gamma_h}\right)\right]-\tan^{-1}\left(\frac{\sqrt{\alpha_h\beta_h}+1\tan(\pi\delta_h)}{\sqrt{\alpha_h}\sqrt{\beta_h}}\right)\right\} \tag{25}$$

On a default channel case in Xcompact3D, the refinement is conducted solely for the

wall-normal direction. In this case, $\gamma_h = 1$ and $\delta_h = \frac{1}{2}$. For all the cases, β_h is set to 0.259065151.

2.3.3 Channel Flow Generalised Richardson Extrapolation Campaign

In order to conduct the Generalised Richardson Extrapolation, several channel flow models must be generated with spatial, temporal, and domain size variation. The variation of the simulation models is shown in Table 4.

Table 4: Simulation Model Variation

Resolution	Finest (FstR)	Fine (FR)	Medium (MR)	Coarse (CR)
L_x	8π	4π	2π	π
L_y	2	2	2	2
L_z	3π	1.5π	0.75π	0.375π
N_x	1024	256	64	16
N_y	1021	509	256	128
N_z	1024	256	64	16
$N_{t,spinup}$	35000	35000	35000	35000
$N_{t,warmup}$	40000	40000	40000	40000
$N_{t,sampling}$	200000	50000	12500	3125
Δt	0.001	0.002	0.004	0.008
t_{tot}	200	100	50	25

Processing the result of the model variation requires a normalised resolution value so the difference in value can be consistently compared. For that, a normalised resolution is introduced as:

$$NR = \frac{\Delta x_e^{current}}{\Delta x_e^{finest}} \frac{\Delta t^{current}}{\Delta t^{finest}} \frac{t_{tot}^{finest}}{t_{tot}^{current}} \frac{L_e^{finest}}{L_e^{current}} \tag{26}$$

Where

$$\Delta x_e = \sqrt[3]{\frac{L_x L_y L_z}{N_x N_y N_z}} \tag{27}$$

$$L_e = \sqrt[3]{L_x L_y L_z} \tag{28}$$

A calculation towards the Asymptotic Grid Convergence Ratio (ASCR) was also done to ensure that the trend is converging to a point. As there are three variations to the mesh resolution, the ASCR value can be calculated as [68]

$$ASCR = \frac{GCI_{23}}{2^p GCI_{12}} \tag{29}$$

Based on the convention [40], the numbering is ordered from the finest to the coarsest mesh resolution. Prior to the above calculation, several parameters must be calculated. The GCI values for neighbouring resolution points are expressed as:

$$GCIi, i+1 = F_s \frac{|(f_i - f_{i+1})|}{2^{\mathcal{P}} - 1} \times 100 \tag{30}$$

F_s is the safety factor, for 3 resolution variation, F_s is set to 1.25 [68]. To calculate the Grid Convergence Index values, the order of convergence should be known using:

$$\mathcal{P} = \frac{\ln\left(\frac{f2-f1}{f2-f1}\right)}{\ln(r)} \tag{31}$$

The grid refinement ratio r is defined using the equation below.

$$r_i = \frac{f_{i+1}}{f_i} \tag{32}$$

After grid convergence is confirmed, the Generalised Richardson Extrapolation can be calculated as:

$$f_{GREP} = f_1 + \frac{f_1 - f_2}{r_1^p - 1} \tag{33}$$

2.3.4 Oscillating Wall Generalised Richardson Extrapolation

Simulating the oscillating wall requires a slight change to the wall boundary condition. By default, the wall is set to a no-slip condition. Therefore, the boundary condition needs to be modified so the wave equation can be included in the wall boundary condition. The base wave equation for the oscillating wall is:

$$w(x,t) = A\sin(2\pi\omega t) \tag{34}$$

For the ease of actuation adjustment in different Reynolds numbers, the wave parameters are non-dimensionalised with wall-normal values [22]. The dimensionless variables required are

$$A^+ = A/u_\tau \tag{35}$$

$$T^+ = 2\pi \frac{u_\tau^2}{\omega\nu} \tag{36}$$

$$k_x^+ = k_x \frac{\nu}{u_\tau} \tag{37}$$

The values of the wall-normalised parameters are based on past studies [9] [69], tabulated in Table 5.

Table 5: Oscillation Parameters Variation

Re	T_{osc}^+	A^+	k_x^+
180	100	4.9	0.0014

For the oscillating wall boundary condition problem, the code must be modified first before compiling, especially for the Navier-Stokes solver, named *navier.f90*. In the said file, the wall z-velocities *uz* for both walls in *pres_correc* subroutine are changed into the defined wall wave function. In this case, the lines 14, 34 and 42 are modified into:

```
!********NCLY==2*************************************
if (ncly1==2) then
    if (xstart(2)==1) then
        do k=1,xsize(3)
            do i=1,xsize(1)
                dpdxy1(i,k)=dpdxy1(i,k)*gdt(itr)
                dpdzy1(i,k)=dpdzy1(i,k)*gdt(itr)
            enddo
        enddo
        do k=1,xsize(3)
            do i=1,xsize(1)
                ux(i,1,k)=byx1(i,k)+dpdxy1(i,k)
                uy(i,1,k)=byy1(i,k)
                uz(i,1,k)=0.31814*sin(2*3.14159*11.18310*t)
            enddo
        enddo
    endif
endif

if (nclyn==2) then
    if (xend(2)==ny) then
        do k=1,xsize(3)
            do i=1,xsize(1)
                dpdxyn(i,k)=dpdxyn(i,k)*gdt(itr)
                dpdzyn(i,k)=dpdzyn(i,k)*gdt(itr)
            enddo
        enddo
    endif
    if (dims(1)==1) then
        do k=1,xsize(3)
```

```
31              do i=1,xsize(1)
32                  ux(i,xsize(2),k)=byxn(i,k)+dpdxyn(i,k)
33                  uy(i,xsize(2),k)=byyn(i,k)
34                  uz(i,xsize(2),k)=0.31814*sin(2*3.14159*11.18310*t)
35              enddo
36          enddo
37      elseif (ny - (nym / dims(1)) == xstart(2)) then
38          do k=1,xsize(3)
39              do i=1,xsize(1)
40                  ux(i,xsize(2),k)=byxn(i,k)+dpdxyn(i,k)
41                  uy(i,xsize(2),k)=byyn(i,k)
42                  uz(i,xsize(2),k)=0.31814*sin(2*3.14159*11.18310*t)
43              enddo
44          enddo
45      endif
46  endif
```

Understanding and quantifying the performance of the flow control method is of utmost importance for this analysis. To calculate the efficiency, the drag reduction is priorly measured using:

$$DR = \frac{\tau_{w,CF} - \tau_{w,osc}}{\tau_{w,CF}} \tag{38}$$

For the net power saving, it is calculated using [9]:

$$NPS = DR - Cost \tag{39}$$

Cost, which is defined as the required power to move the wall can be calculated using:

$$Cost_{osc} = \frac{1}{p_{CF} T_{av} L_x L_y} \int_{t_i}^{t_f} \int_0^{L_x} \int_0^{L_z} w \tau_z dx dz dt \tag{40}$$

It is important to note that finest resolution models are not used in the study of the spanwise oscillating wall flow control. This is carried out in order to evaluate the effectiveness of the Generalised Richardson Extrapolation and to reduce simulation costs.

3 Results and Discussion

3.1 Laminar Flow Around a Cylinder Case Results

A test case of laminar flow around a cylinder is generated to test the effectivity of the Xcompact3D code. The resulting velocity contour of the flow around the cylinder is shown in Figure 5.

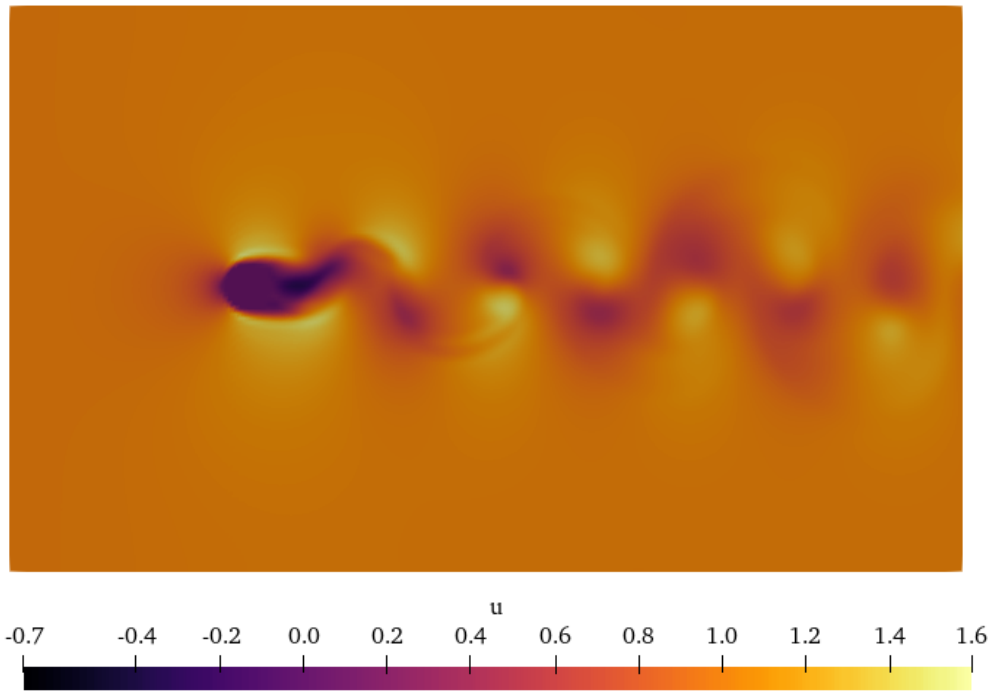

Figure 5: The u Velocity of A Laminar Flow Past a Cylinder, with the von Karman Vortex Street Visible in the Wake

As seen, there is a repeating and alternating pattern of vortices behind the cylinder. This is generally known as the von Karman vortex street. This phenomenon occurs when a bluff body is subjected through a flow in certain Reynolds number ranges, which detaches and creates the said vortex shedding behaviour [70]. For a fully turbulent vortex street, it occurs within the range of Re = 300 to 3×10^5 [71], which is what occurs in this case.

The value of flow properties of the case can also be calculated using the default Py4Incompact3D environment, which resulted in Figure 6.

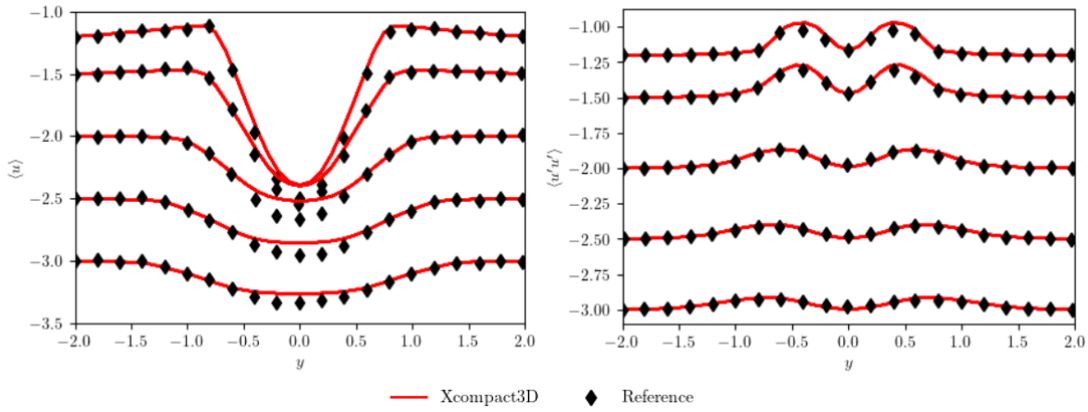

Figure 6: Mean Velocity and Velocity RMS Profile for the Cylinder Wake Flow, the Reference Corresponds with Mittal and Balanchandar Data [72]

The mean velocity and velocity RMS profile are then compared to the reference result [72]. Based on the plots, it can be seen that the mean and fluctuating u-velocity result generated by Xcompact3D has a decent agreement with the reference results. Therefore, it validates the performance of Xcompact3D, proving it is a decent tool to use for simulating turbulent flows.

3.2 Channel Flow Results

3.2.1 Simulation Metrics

The simulation of several mesh resolutions has been generated. The time, memory and computational requirement of the simulation is shown at 6. Based on the table, the finest mesh simulation requires an excessive amount of time and resources. These requirements, especially the time requirement, do not seem to be decreased by the speedup in the ARCHER2 environment. The most probable cause for the phenomenon is the code structures, which may hinder significant speedup from the increased number of cores in the HPC environment.

Table 6: Resources Requirement for Various Mesh Resolutions

Resolution	Finest (FstR)	Fine (FR)	Medium (MR)	Coarse (CR)
Maximum Number of Cores	2048	512	256	128
Simulation Time (h)	≈ 182	≈ 7	≈ 0.232	≈ 0.00028
Memory Requirement (MiB)	76007.843	2422.332	76.580	2.422

The resource requirement table also highlights the importance of the usage of Generalised Richardson Extrapolation. If the extrapolation works as intended, then the computational requirement can be significantly reduced. By only running the coarse, medium, and fine

resolution, the simulation time can be reduced by 96.026% relative to running the finest resolution case, and the memory requirement can be reduced by 96.683%. Therefore, the computational limitation can be pushed if Generalised Richardson Extrapolation is used.

3.2.2 Coefficient of Friction Result

A parameter of the simulation results is used to determine the ideal and converged simulation result using the Generalised Richardson Extrapolation. The coefficient of friction parameter in various resolutions is used in the grid convergence study. To validate the convergence of the analysis, the ASCR value must be calculated with the results as follows:

Table 7: Grid Convergence Parameters

$\mathcal{P}$	GCI_{12}	GCI_{23}	ASCR
0.392257	1.746708	4.596836	1.028421

Based on the results, it is apparent that the resolution values are already sufficient to show a converging value in the channel flow simulations. Because of that, the Generalised Richardson Extrapolation value can be determined, with results shown in Figure 2.3.

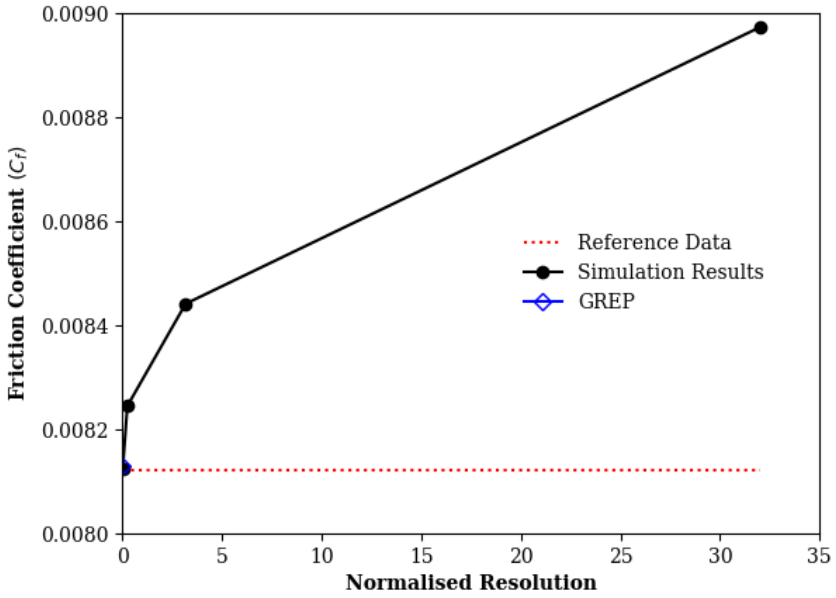

Figure 7: Coefficient of Friction Results of Different Mesh Resolution Models Combined With Generalised Richardson Extrapolation Results

Based on the figure, the value of the finest mesh resolution is observed to nearly coincide with reference data given [73]. Additionally, the fine resolution is already quite close to the reference data. This is a promising result as it can suggest that the fine resolution values are adequate to simulate channel flows streamwise velocity profile at $Re_\tau = 180$, decreasing the computational requirement.

For the Generalised Richardson extrapolation, the result is nearly identical to the reference data and the finest resolution model, only yields 0.00093% difference to the reference value and 0.00046% error to the finest resolution model results. Therefore, the proposed Generalised Richardson Extrapolation can be deemed as a valid and sufficient model to predict the values of the coefficient of friction in an ideal resolution.

3.2.3 Mean Streamwise Velocity

Figure 8 displays the mean streamwise velocity of the channel flow normalised to the viscous length scale.

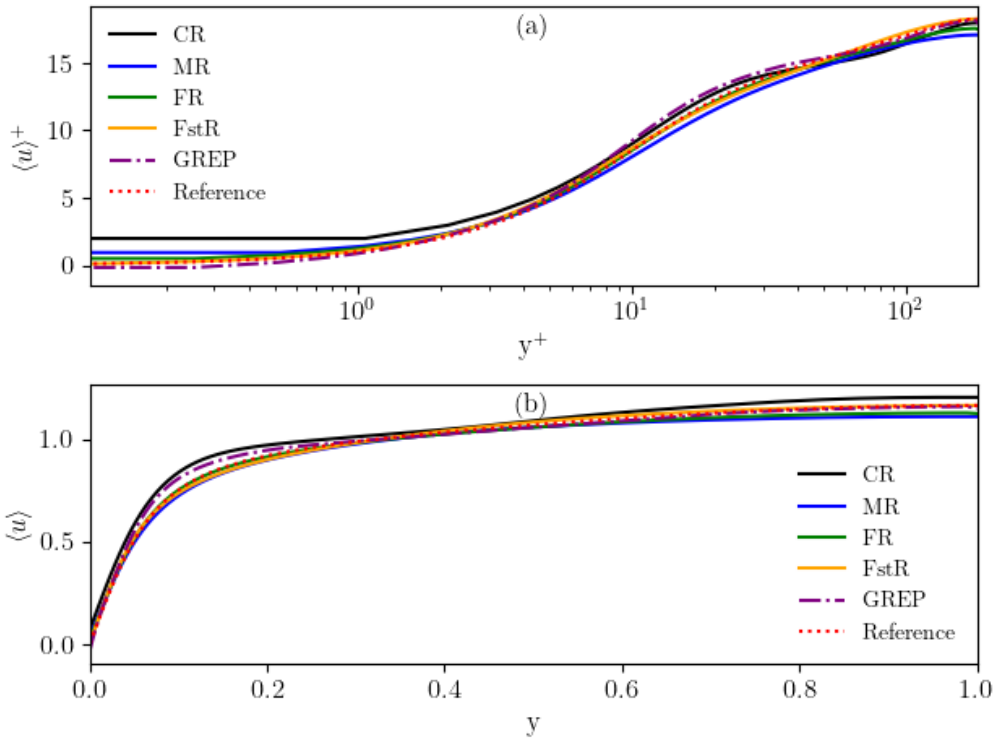

Figure 8: Mean Streamwise Velocity (a) as a Function of Viscous Length Scale and (b) As It Is, on the First Half of the Height of the Channel Flow. The Reference Data Corresponds with Lee and Moser Channel Flow Data [73]

Overall, the results are generated as expected, as all of the velocity trends follow the law of the wall. The similarity within the trends means that the boundary layer in the flow is correctly captured in all regions. The first region from the left-hand side is the linear sublayer, ranging at $y^+ \leq 7$ [74] and has a linear increase to the velocity. The second is the buffer layer, which is located at $7 \leq y^+ \leq 40$, visually distinct as the velocity profile is drastically changed. This region is strongly turbulent, which is the main source of the turbulence that will be transported to the outer layer afterwards [75]. Lastly is the log-law region, in which the trend is commonly described by a logarithm sequence [76]. This region ranges from $y^+ = 40$ afterwards.

Comparing the results from different resolution models, it is visible that the velocity values are gradually becomes closer to the reference result as the resolution becomes more detailed. Both fine and the finest resolution models have an excellent agreement with the reference velocity contour with inaccuracies only at the centre of the channel domain.

The satisfactory result of the fine resolution model translates to the result of Generalised Richardson Extrapolation, which is also observed to have a decent result relative to the reference values. Generalised Richardson Extrapolation is seen to eliminate the inaccuracies on the centre of the flow, creating a more accurate line on $y^+ > 10^2$. However, the Generalised Richardson Extrapolation result suffers a considerable amount of inaccuracies, most observable in the buffer zone. This can be observed as the consequence of inaccurate coarse resolution model results. Due to its large cell size, the turbulence within the buffer zone is not captured correctly, creating results that are far from the reference values. The inaccurate values then affect the Generalised Richardson Extrapolation result, which takes the coarse resolution model into account.

3.2.4 Reynolds Stresses

Reynolds stress tensor comprised of six different unique elements. The non-zero elements of the Reynolds stress tensor of a channel flow are comprised of three normal stress values and one shear stress value. The normal stress values are the diagonal members of the Reynolds stress tensor, denoted by $\langle u'u' \rangle$, $\langle v'v' \rangle$, and $\langle w'w' \rangle$. The difference in these values signifies the anisotropic nature of the turbulent flow. These variables also show the value of turbulent kinetic energy, which displays the energy in the flow turbulent fluctuations. The last non-zero member, $\langle u'v' \rangle$, denotes the shear stress within the flow. The value of the member is not zero due to the interaction between the mean streamwise flow with the wall-normal boundary layer flow. The value of the shear stress highly correlates with the mixing and momentum exchange between different layers of the fluid.

For the two other Reynolds stress tensor members, namely $\langle u'w' \rangle$, $\langle v'w' \rangle$, the value is zero. This is because there is no velocity in the wall-normal and spanwise direction, thus making zero interactions between those velocities. However, in most cases, the results from the simulation might not be exactly zero due to truncation error. The resulting Reynolds stress component values are shown in Figure 9.

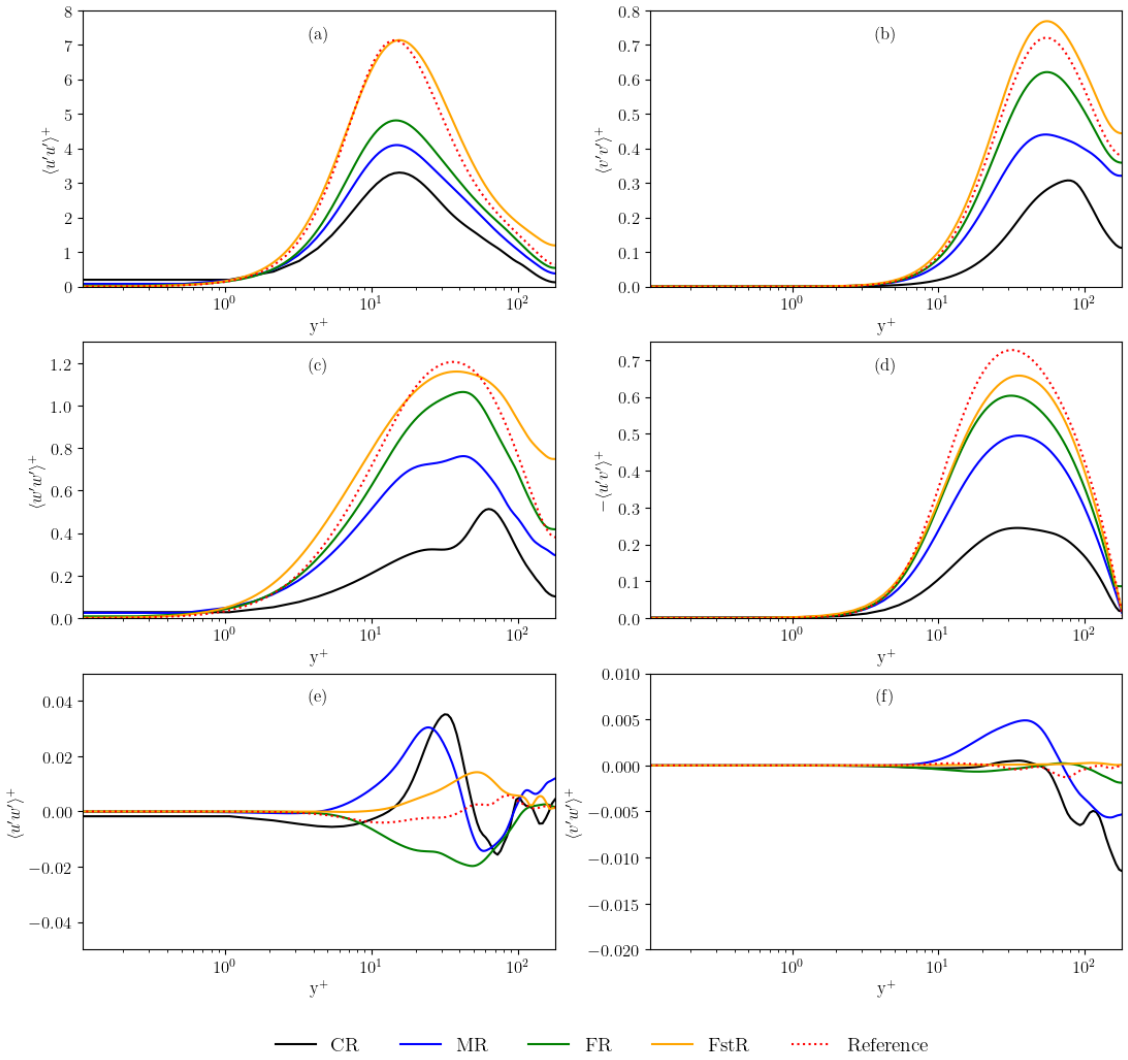

Figure 9: Reynolds Stress Tensor Components, Normalised with Viscous Terms: a) Streamwise Component, b) Wall-Normal Component, c) Spanwise Component, d) Covariance of Streamwise and Wall-Normal Component, e) Convariance of Streamwise and Spanwise Component, and f) Covariance of Wall-Normal Component and Spanwise Component. The Values Are Compared to the Reference Data [73]

A significant discovery is made regarding the $\langle u'u' \rangle$ values plot. The fine and finest resolution findings show a large difference in value. Upon analysing the flow phenomenon, it was discovered that this is caused by turbulence capturing by the grids. Research has revealed that in the streamwise direction, the $\langle u'u' \rangle$ values are altered by the large-scale turbulence on the boundary layer's outer region, which modifies the small-scale amplitude [77]. When the spatial resolution is inadequate, the stretching causes the large-scale turbulence to be incorrectly caught by the flow, which in turn causes the modulation effect by the large scale to be incorrectly captured. This substantially lowers the $\langle u'u' \rangle$ value.

Observing the overall result of the Reynolds stress tensor members, it is evident that the

values of non-zero members are increasingly closer to the reference value as the resolution increases. However, Reynolds stress tensor components results also show that the coarse, medium and fine resolution results can not show an acceptable result which can reflect the actual physics of the flow. Only results from the finest resolution can sufficiently match the reference values.

Other than displaying the inadequacy of the coarse, medium and fine result, the second-order statistics such as the Reynolds stress tensor can also show the limitation of the Generalised Richardson Extrapolation, shown in Figure 10.

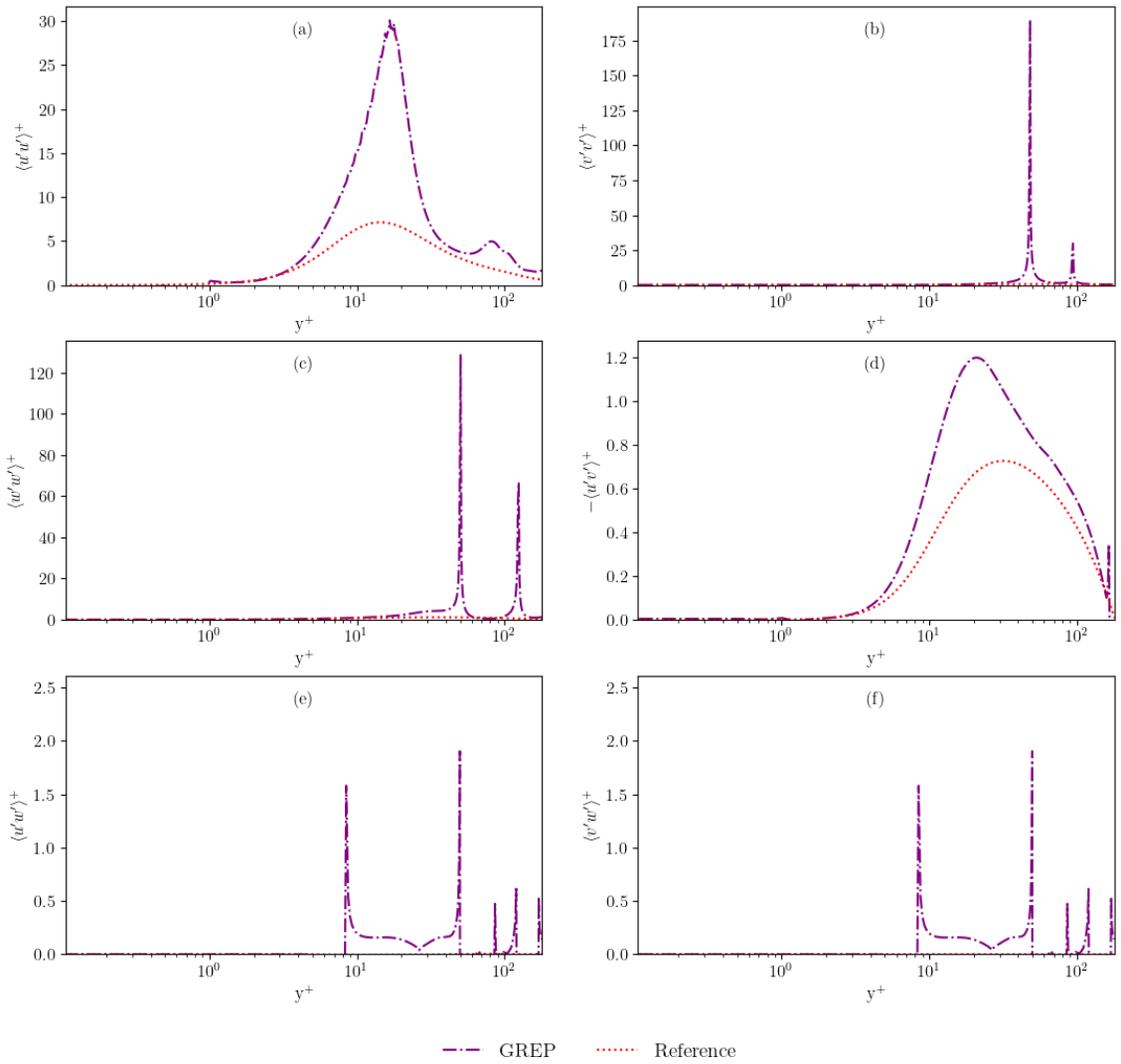

Figure 10: Generalised Richardson Extrapolation of the Reynolds Stress Tensor Terms, Normalised with Viscous Terms: a) Streamwise Component, b) Wall-Normal Component, c) Spanwise Component, d) Covariance of Streamwise and Wall-Normal Component, e) Convariance of Streamwise and Spanwise Component, and f) Covariance of Wall-Normal Component and Spanwise Component. The Values Are Compared to the Reference Data [73]

As shown in the figure, the results of the Generalised Richardson Extrapolation are very

distant from the reference values. By analysing the calculation process, these errors are caused by two main reasons. First is the diverging results of some points in the plots. The diverging result caused an error in the Generalised Richardson Extrapolation algorithm and overestimated the idealised value.

The second reason is the slow rate of convergence. As seen in the graph, some points have the same distance between coarse and medium values as well as the medium and the fine values. Consequently, the slow rate of convergence affects the order of convergence p, thus affecting the Generalised Richardson Extrapolation result. Because of these reasons, the Generalised Richardson Extrapolation is unusable for approximating the ideal value of Reynolds stress tensor components.

3.3 Oscillating Wall Flow Control

3.3.1 Simulation Metrics

After generating the oscillating wall flow control simulation, the simulation requirements can be summarised. The requirements for running the simulations are displayed in Figure 8.

Table 8: Resources Requirement for Various Mesh Resolutions for the Oscillating Wall Boundary Condition

Resolution	Fine (FR)	Medium (MR)	Coarse (CR)
Maximum Number of Cores	512	256	128
Simulation Time (h)	≈ 7	≈ 0.250	≈ 0.00032
Memory Requirement (MiB)	2422.332	76.580	2.422

The time required for running an oscillating wall flow control is observed to be higher. This is due to the additional calculation of the changing boundary condition value. However, the change is minuscule due to the code efficiency.

3.3.2 Coefficient of Friction Results

The result of the coefficient of friction of the oscillating wall flow control is shown in Figure 11. The decrease of friction inside the channel flow is observed in the plot. This proves the effect of the flow control has been positive for the flow case.

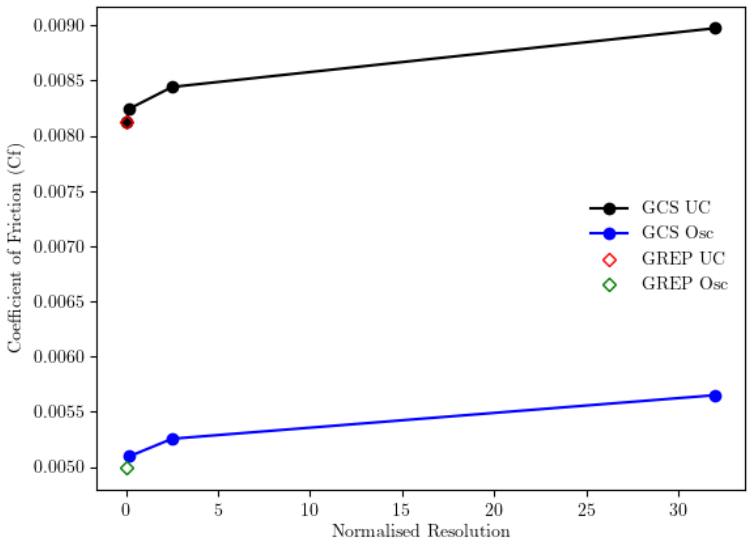

Figure 11: Coefficient of Friction Results of Uncontrolled Channel Flow and Oscillating Wall Flow Control Applied

Since both DR and cost depend on wall shear stress, the performance metrics of a flow control technique can be computed from the coefficient of friction. The performance comparison between the reference values and the simulated case is shown in Table 9.

Table 9: Oscillating Wall Flow Control Performance, Compared with Reference Data [69]

Metrics	DR(%)	Cost(%)	NPS(%)
GREP	39.4	136	-96.6
Reference	41.3	142	-100

Both the reference and the Generalised Richardson Extrapolation results have shown consistent results, with the extrapolation slightly underestimating the values. As the reference suggests, the result shows what is expected in applying large amplitude on a spanwise oscillating wall flow control case. Using a large amplitude, the system exhibits a sufficient drag reduction performance. However, the power required becomes too high, eliminating any power-saving benefits in the system [9][69]. Therefore, the flow control setup is not economically practical enough to employ in a channel flow case with Re $\approx$ 180.

3.3.3 Mean Streamwise Velocity

The mean streamwise velocity is calculated for the oscillating channel flow case, shown in Figure 12. The results are compared to the simple channel flow reference case to visualise the behaviour difference in the flow.

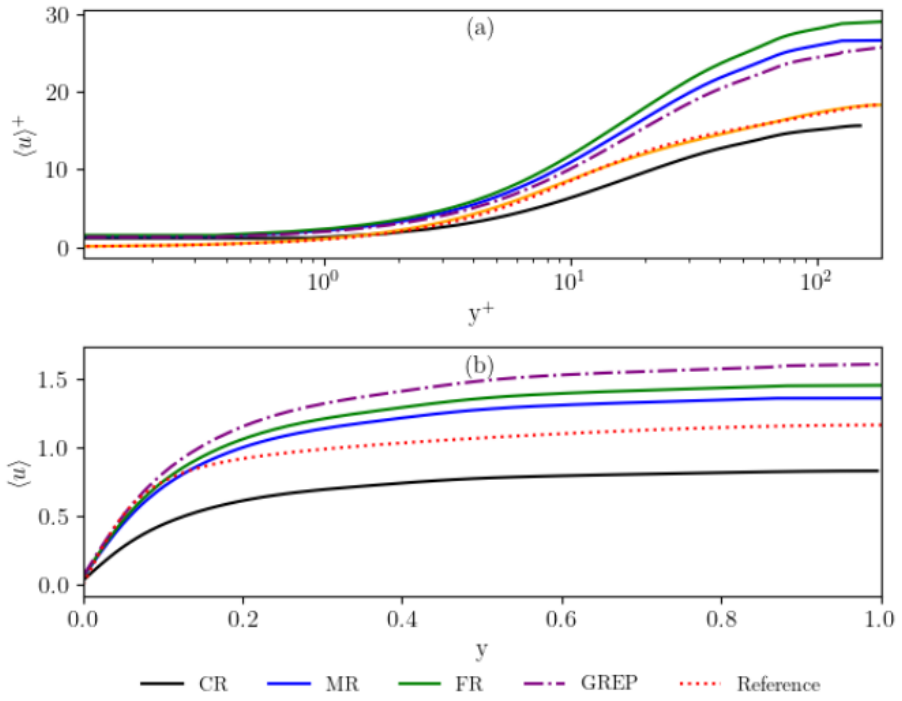

Figure 12: Mean Streamwise Velocity (a) as a Function of Viscous Length Scale and (b) As It Is, on the First Half of the Height of the Channel Flow with Spanwise Oscillating Wall Flow Control. The Result is Compared to Simple Channel Flow Data [73]

The behaviour of the Generalised Richardson Extrapolation results for the oscillating wall channel flow cases has been fairly consistent with the simple channel flow cases in Figure 8. The velocity profile results of the coarse, medium and fine resolution model have converged to sensible points, which makes the Generalised Richardson Extrapolation employable for predicting the said results. The sensibility of the results can be applied to the reference value in which the spanwise oscillating channel flow is applied in the same flow regime [69].

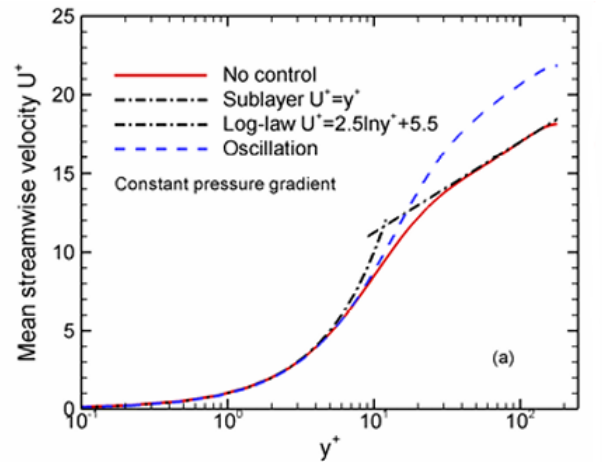

Figure 13: Reference Wall Normal Velocity Value [69]

A similar result can be observed when comparing Figure 12 and 13. The velocity gradient on the log-law region is seen to be increased compared to the simple channel flow case. This is a characteristic of a flow control case, caused by the increase of viscous sublayer thickness [78][79]. However, as shown in Table 9, the DNS simulation underestimates the results of flow control, which caused a lower increase in velocity profile slope.

3.3.4 Reynolds Stresses

The addition of spanwise oscillation changes the flow behaviour in the channel flow, thus affecting the value of the Reynolds stress tensor components. The result of the Reynolds stress components is shown in Figure 14.

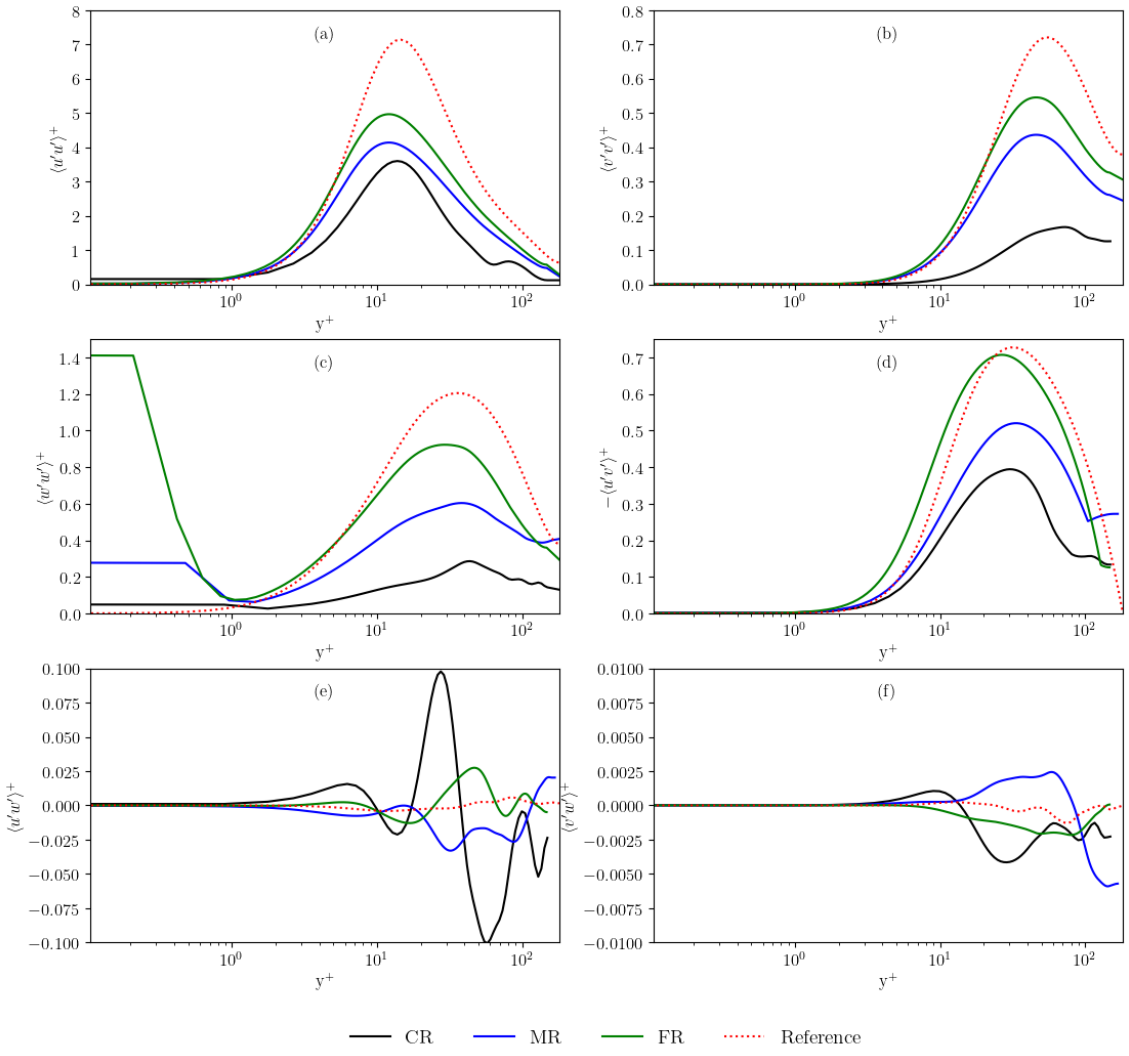

Figure 14: Reynolds Stress Tensor Components of the Spanwise Oscillating Flow Control Case, Normalised with Viscous Terms: a) Streamwise Component, b) Wall-Normal Component, c) Spanwise Component, d) Covariance of Streamwise and Wall-Normal Component, e) Convariance of Streamwise and Spanwise Component, and f) Covariance of Wall-Normal Component and Spanwise Component. The Values Are Compared to the Reference Simple Channel Flow Data [73]

Between the result of Reynolds stresses of the basic channel flow and the result produced by the channel flow with spanwise oscillating flow control, three important conclusions can be inferred. The first point relates to the change of values in the components related to spanwise velocity fluctuation. For $\langle w'w' \rangle$ component, the value near the wall significantly jumped due to the oscillations. Additionally, the oscillation increased the interaction between the spanwise and streamwise velocity, increasing the value of $\langle u'w' \rangle$. Conversely, as the spanwise oscillation purposed to decrease the instability on the wall-normal velocities, the value of $\langle v'w' \rangle$ decreases.

The results of non-zero Reynolds stress tensor members in channel flows are somewhat pushed to the left of the graphs, which is the second inference that can be made from the picture. This is typical in spanwise oscillating wall flow control cases, where turbulence suppression is presented. The attenuation, in turn, leads to values redistribution of the Reynolds stresses [80].

The third point is that the simulation findings do not show any noteworthy changes, despite the fact that a number of references displayed lower overall Reynolds stresses in comparison to the basic channel flow cases [79][80]. Although this appears to be an unusual and undesired result to produce in flow control instances, the reference results [69] verifies this study's results. The main reason for this phenomenon is the use of a constant pressure gradient (CPG) to define the boundary condition in the periodic planes of the channel flow. Because of the CPG setting, the pressure is fixed while the flow rate value is dependent on the drag within the system. In a reduced drag system such as the spanwise oscillating wall flow control cases, the flow rate increases due to the constant pressure gradient as the driving force. The increased flow rate adjusts the overall Reynolds stresses [81]. Because of this, the Reynolds stress components remain constant when normalised.

The Generalised Richardson Extrapolation for predicting the ideal values of Reynolds stresses yields the same behaviour as the simple channel flow result mentioned in Section 3.2.4. All of the results are extremely overestimated, rendering the Generalised Richardson Extrapolation results unusable. The result of extrapolated Reynolds stress members is shown in Figure 15.

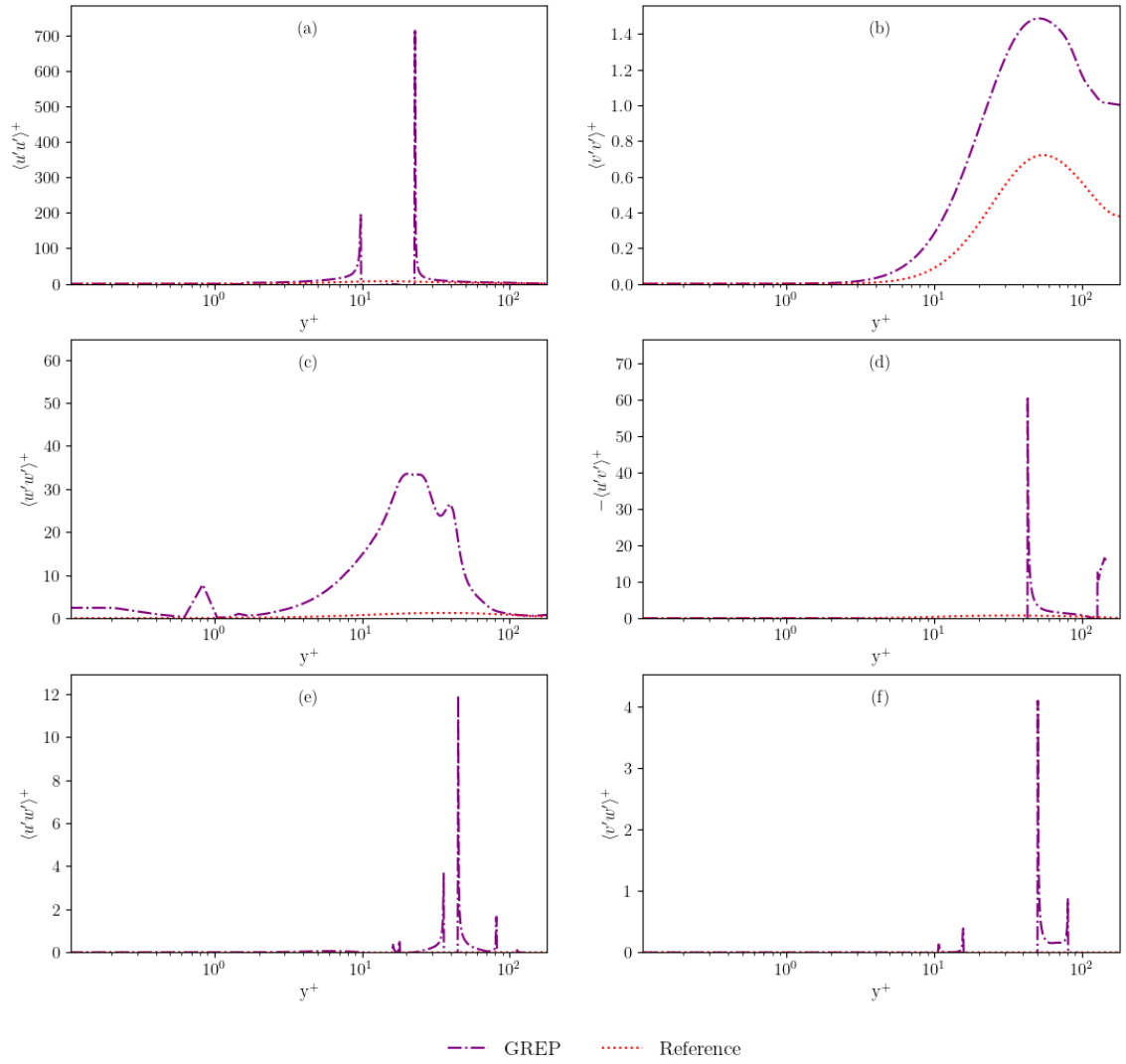

Figure 15: Generalised Richardson Extrapolation of the Reynolds Stress Tensor Components in the Channel Flow with Spanwise Oscillating Wall Flow Control, Normalised with Viscous Terms: a) Streamwise Component, b) Wall-Normal Component, c) Spanwise Component, d) Covariance of Streamwise and Wall-Normal Component, e) Convariance of Streamwise and Spanwise Component, and f) Covariance of Wall-Normal Component and Spanwise Component. The Values Are Compared to the Reference Data [73]

3.3.5 Instantaneous Velocity Fields

The contours can also be examined to further enforce the reasoning inside of previous findings. The resulting instantaneous velocity contour of the simple channel flow and the channel flow with spanwise oscillating wall flow control is shown in Figure 16. For an equal comparison and a sensible result, the fine resolution of both cases is used for this analysis.

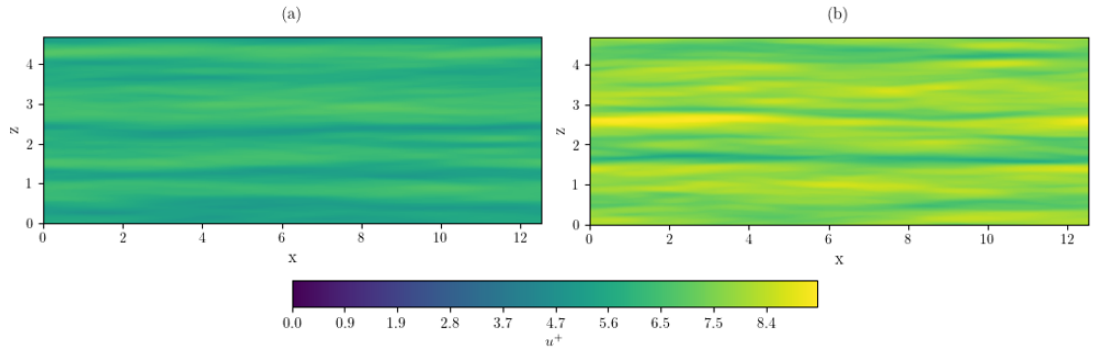

Figure 16: Instantaneous Velocity Contour of Simple Channel Flow and Channel Flow with Spanwise Oscillating Flow Control at t = 100 and y+ = 10, Normalised with Viscous Terms

The figure highlights the streamwise velocity streaks inside the channel flow. These streaks are the hallmarks of the coherent structures inside the flow. As evident in the figure, the velocity of the streak increases when the spanwise oscillating wall flow control is applied. This enforces the argument of the effect of constant pressure gradient settings in Section 3.3.4. Due to the application of the flow control, the drag inside the system decreases. This, in turn, increases the velocity inside the channel flow.

Additionally, the length of the low-speed streaks for the region with spanwise oscillating wall flow control applied is observed to be shorter than the simple channel flow case. One of the examples in the Figure is the streak within $z \approx 0.5$. In simple channel flow, the streak spans the entire streamwise length with approximately the same velocity. However, on the spanwise oscillating channel flow case, the low velocity streak is seen to be diminishing, as the effect of the flow control application. This agrees with the finding from reference [69].

4 Conclusions and Recommendations

4.1 Conclusions

The study of Generalised Richardson Extrapolation in a canonical channel flow and an oscillating wall channel flow is successfully conducted. All of the analysis has been successfully conducted in ARCHER2 and CRESCENT2 HPC environments with Xcompact3D as the simulation software.

Overall, Generalised Richardson Extrapolation results have been promising. The resources required to generate the Generalised Richardson Extrapolation are shown to be significantly smaller than simulating the flow at the acceptable resolution values based on references. Additionally, Generalised Richardson Extrapolation velocity contour and coefficient of friction results generated an excellent agreement towards the reference results. However, for generating the ideal value for second-order statistics such as Reynolds stress tensor components, the current Generalised Richardson Extrapolation method has not been useful as overestimation occurs at every point.

Oscillating wall flow control has also been applied to the channel flow cases, with noticeable improvement relative to the simple channel flow case. The velocity gradient is observed to increase at log-layer and beyond. The drag is also seen to be significantly smaller with the wall oscillation settings. However, enforcing the finding in the references, there is no positive net power saving generated when the setting is applied as the amplitude is set too high. In addition, Generalised Richardson Extrapolation also has been successfully applied to the spanwise oscillating wall flow control cases with the same quality of results as the simple channel flow.

4.2 Recommendations for Future Work

In this study, multiple occurrences of recompiling are done to modify the wall boundary condition. This is done due to the wall boundary condition being hard-coded into the simulation subroutine. To create a more efficient workflow between cases with and without oscillating wall flow control, it is recommended to create a system within the Xcompact3D source code where an additional input file is involved. The input file is filled with the desired velocity boundary condition to the streamwise, spanwise, and wall-normal directions. This way, the entire Xcompact3D software will only need to be compiled once.

For future studies of Generalised Richardson Extrapolation of oscillating wall flow control cases, it is important to expand the study to higher Reynolds numbers. It is known that a high Reynolds number case requires more computational resources, therefore giving more challenge to the Generalised Richardson Extrapolation algorithm. This also can

open more information towards the performance of oscillating wall flow control, which was rarely done before.

Other variations of Generalised Richardson Extrapolation can also be applied to test the range of the method. For example, by maintaining the computational domain size and varying the others, the effectivity of the Generalised Richardson Extrapolation can be analysed.

4.3 Technical Acknowledgement

The author would like to thank the EPCC and UK Turbulence Consortium for providing ARCHER2 computing resources (grant number EP/D44073/1; EP/G06958/1). Additional computing time was also provided by Cranfield University in CRESCENT2 HPC environment. Finally, the author would like to thank Dr. Sylvain Laizet and Dr. Paul Bartholomew for their immense support towards the application of Xcompact3D and Py4Incompact3D.

References

[1] E. Douglas, J. Jacobs, K. Hayhoe, *et al.*, "Progress and challenges in incorporating climate change information into transportation research and design," *Journal of Infrastructure Systems*, vol. 23, no. 4, p. 04 017 018, 2017. DOI: 10.1061/(ASCE)IS.1943-555X.0000377. eprint: https://ascelibrary.org/doi/pdf/10.1061/%28ASCE%29IS.1943-555X.0000377. [Online]. Available: https://ascelibrary.org/doi/abs/10.1061/%28ASCE%29IS.1943-555X.0000377.

[2] Met Office, *Causes of climate change*. [Online]. Available: https://www.metoffice.gov.uk/weather/climate-change/causes-of-climate-change.

[3] IRENA, *Investment Needs of USD 35 trillion by 2030 for Successful Energy Transition*, 2023. [Online]. Available: https://www.irena.org/News/pressreleases/2023/Mar/Investment-Needs-of-USD-35-trillion-by-2030-for-Successful-Energy-Transition.

[4] IEA, *Tracking clean energy progress 2023*. [Online]. Available: https://www.iea.org/reports/tracking-clean-energy-progress-2023.

[5] A. Abbas, G. Bugeda, E. Ferrer, *et al.*, "Drag reduction via turbulent boundary layer flow control," *Science China Technological Sciences*, vol. 60, pp. 1281–1290, 9 Sep. 2017, ISSN: 18691900. DOI: 10.1007/s11431-016-9013-6.

[6] C. Airiau, R. King, and B. R. Noack, *Open invited track : Flow control strategies and applications*, 2016.

[7] R. Benzi and F. Toschi, "Lectures on turbulence," *Physics Reports*, vol. 1021, pp. 1–106, Jun. 2023, ISSN: 03701573. DOI: 10.1016/j.physrep.2023.05.001.

[8] W. Bell, "The influence of turbulence on drag," *Ocean Engineering*, vol. 6, pp. 329–340, 3 Jan. 1979, ISSN: 00298018. DOI: 10.1016/0029-8018(79)90021-0.

[9] I. Marusic, D. Chandran, A. Rouhi, *et al.*, "An energy-efficient pathway to turbulent drag reduction," *Nature Communications*, vol. 12, 1 Dec. 2021, ISSN: 20411723. DOI: 10.1038/s41467-021-26128-8.

[10] T. Alberti, R. Benzi, and V. Carbone, "Why (still) studying turbulence in fluids and plasmas?" *Perspectives of Earth and Space Scientists*, vol. 4, 1 Dec. 2023, ISSN: 2637-6989. DOI: 10.1029/2023cn000215.

[11] S. Chen, S. Sammak, P. Givi, J. P. Yurko1, and X. Jia, "Reconstructing high-resolution turbulent flows using physics-guided neural networks," Sep. 2021. [Online]. Available: http://arxiv.org/abs/2109.03327.

[12] K. R. Sreenivasan, "Fluid turbulence," *Reviews of Modern Physics*, vol. 71, pp. 383–395, 2 1999.

[13] A. K. F. Hussain, "Coherent structures and turbulence," *Journal of Fluid Mechanics*, vol. 173, pp. 303–356, 1986, ISSN: 14697645. DOI: 10.1017/S0022112086001192.

[14] H. E. Fiedler, "Coherent structures in turbulent flows," *Prog. Aerospace Sci.*, vol. 25, pp. 231–269, 1988.

[15] Y. Wang, W. Huang, and C. Xu, "On hairpin vortex generation from near-wall streamwise vortices," *Acta Mechanica Sinica/Lixue Xuebao*, vol. 31, pp. 139–152, 2 May 2015, ISSN: 05677718. DOI: 10.1007/s10409-015-0415-8.

[16] T. I. Józsa, *Drag reduction by passive in-plane wall motions in turbulent wall-bounded flows[ph.d thesis]*, 2019.

[17] G. Alfonsi, "Coherent structures of turbulence: Methods of eduction and results," *Applied Mechanics Reviews*, vol. 59, pp. 307–323, 1-6 2006, ISSN: 00036900. DOI: 10.1115/1.2345370.

[18] Y. Fan and W. Li, "Spectral analysis of turbulence kinetic and internal energy budgets in hypersonic turbulent boundary layers," *Phys. Rev. Fluids*, vol. 8, p. 044 604, 4 Apr. 2023. DOI: 10.1103/PhysRevFluids.8.044604. [Online]. Available: https://link.aps.org/doi/10.1103/PhysRevFluids.8.044604.

[19] C. Brennen, "Turbulence spectra and scales," in California Institute of Technology, 2004.

[20] T. Kalmár-Nagy and B. D. Bak, "An intriguing analogy of kolmogorov's scaling law in a hierarchical mass–spring–damper model," *Nonlinear Dynamics*, vol. 95, pp. 3193–3203, 4 Mar. 2019, ISSN: 0924-090X. DOI: 10.1007/s11071-018-04749-x.

[21] M. Jahamiri, *Active flow control: A review*, 2010.

[22] P. Ricco, M. Skote, and M. A. Leschziner, "A review of turbulent skin-friction drag reduction by near-wall transverse forcing," *Progress in Aerospace Sciences*, vol. 123, May 2021, ISSN: 03760421. DOI: 10.1016/j.paerosci.2021.100713.

[23] D. Gatti and M. Quadrio, "Reynolds-number dependence of turbulent skin-friction drag reduction induced by spanwise forcing," *Journal of Fluid Mechanics*, vol. 802, pp. 553–582, Sep. 2016, ISSN: 14697645. DOI: 10.1017/jfm.2016.485.

[24] M. Quadrio, P. Ricco, and C. Viotti, "Streamwise-travelling waves of spanwise wall velocity for turbulent drag reduction," *Journal of Fluid Mechanics*, vol. 627, pp. 161–178, 2009, ISSN: 14697645. DOI: 10.1017/S0022112009006077.

[25] F. Auteri, A. Baron, M. Belan, G. Campanardi, and M. Quadrio, "Experimental assessment of drag reduction by traveling waves in a turbulent pipe flow," *Physics of Fluids*, vol. 22, 115103 Aug. 2010. DOI: 10.1063/1.3491203. [Online]. Available: http://arxiv.org/abs/1008.2584%20http://dx.doi.org/10.1063/1.3491203.

[26] C. Viotti, M. Quadrio, and P. Luchini, "Streamwise oscillation of spanwise velocity at the wall of a channel for turbulent drag reduction," *Physics of Fluids*, vol. 21, pp. 1–9, 11 2009, ISSN: 10706631. DOI: 10.1063/1.3266945.

[27] D. Chandran, A. Zampiron, A. Rouhi, *et al.*, "Turbulent drag reduction by spanwise wall forcing. part 2. high-reynolds-number experiments," *Journal of Fluid Mechanics*, vol. 968, Jul. 2023, ISSN: 14697645. DOI: 10.1017/jfm.2023.498.

[28] R. Deshpande, A. G. Kidanemariam, and I. Marusic, "Pressure drag reduction via imposition of spanwise wall oscillations on a rough wall," *Journal of Fluid Mechanics*, vol. 979, Jan. 2024, ISSN: 0022-1120. DOI: 10.1017/jfm.2023.1062.

[29] V. T. Nguyen, P. Ricco, and G. Pironti, "Separation drag reduction through a spanwise oscillating pressure gradient," *Journal of Fluid Mechanics*, vol. 912, 2021, ISSN: 14697645. DOI: 10.1017/jfm.2020.1124.

[30] P. Ricco, C. Ottonelli, Y. Hasegawa, and M. Quadrio, "Changes in turbulent dissipation in a channel flow with oscillating walls," *Journal of Fluid Mechanics*, vol. 700, pp. 77–104, Jun. 2012, ISSN: 14697645. DOI: 10.1017/jfm.2012.97.

[31] D. D. Apsley, *Flow in Pipes and Channels [Lecture Notes]*, 2023. [Online]. Available: https://personalpages.manchester.ac.uk/staff/david.d.apsley/lectures/hydraulics2/t2.

[32] The TrEnCh Project, "Turbulence and fluid flow," in University of Washington, 2023.

[33] K. Duraisamy, G. Iaccarino, and H. Xiao, "Turbulence modeling in the age of data," *Annual Review of Fluid Mechanics*, vol. 51, pp. 357–377, 1 Jan. 2019, ISSN: 0066-4189. DOI: 10.1146/annurev-fluid-010518-040547.

[34] N. A. C. Sidik, S. N. A. Yusuf, Y. Asako, S. B. Mohamed, and W. M. A. A. Japa, "A short review on rans turbulence models," *CFD Letters*, vol. 12, pp. 83–96, 11 Nov. 2020, ISSN: 21801363. DOI: 10.37934/cfdl.12.11.8396.

[35] R. H. Bush, T. Chyczewski, K. Duraisamy, B. Eisfeld, C. L. Rumsey, and B. R. Smith, *Recommendations for future efforts in rans modeling and simulation*, 2020.

[36] Y. Zhiyin, "Large-eddy simulation: Past, present and the future," *Chinese Journal of Aeronautics*, vol. 28, pp. 11–24, 1 Feb. 2015, ISSN: 10009361. DOI: 10.1016/j.cja.2014.12.007.

[37] P. Mason, "Large-eddy simulation: A critical review of the technique," *Quarterly Journal of Royal Meteorological Society*, vol. 120, pp. 1–26, 1994.

[38] P. Moin and K. Mahesh, "Direct numerical simulation: A tool in turbulence research," *Annual Review of Fluid Mechanics*, vol. 30, pp. 539–578, 1998, ISSN: 00664189. DOI: 10.1146/annurev.fluid.30.1.539.

[39] J. Boschung, F. Hennig, M. Gauding, H. Pitsch, and N. Peters, "Generalised higher-order kolmogorov scales," *Journal of Fluid Mechanics*, vol. 794, pp. 233–251, May 2016, ISSN: 14697645. DOI: 10.1017/jfm.2016.172.

[40] P. Roache, "Verification and validation in computational science and engineering," *Journal of Computational Physics*, vol. 123, no. 4, pp. 567–589, 2009.

[41] C. E. Groves, M. Ilie, and P. Schallhorn, *Comprehensive approach to verification and validation of cfd simulations applied to backward facing step - application of cfd uncertainty analysis*, 2012.

[42] P. Bartholomew, G. Deskos, R. A. Frantz, F. N. Schuch, E. Lamballais, and S. Laizet, "Xcompact3d: An open-source framework for solving turbulence problems on a cartesian mesh," *SoftwareX*, vol. 12, Jul. 2020, ISSN: 23527110. DOI: 10.1016/j.softx.2020.100550.

[43] S. Laizet, "Incompact3d: A powerful tool to tackle turbulence problems on supercomputers," T. Kvamsdal, Ed., 2014. [Online]. Available: http://www3.imperial.ac.uk/tmfc/people/sylvainlaizet/.

[44] S. Laizet and E. Lamballais, "High-order compact schemes for incompressible flows: A simple and efficient method with quasi-spectral accuracy," *Journal of Computational Physics*, vol. 228, pp. 5989–6015, 16 Sep. 2009, ISSN: 10902716. DOI: 10.1016/j.jcp.2009.05.010.

[45] Cornell University, *Scaling [virtual workshop note]*, 2024. [Online]. Available: https://cvw.cac.cornell.edu/parallel/efficiency/scaling.

[46] X. Li, *Scalability: Strong and weak scaling*, 2018. [Online]. Available: https://www.kth.se/blogs/pdc/2018/11/scalability-strong-and-weak-scaling/.

[47] G. M. Amdahl, "Validity of the single processor approach to achieving large scale computing capabilities," in *Proceedings of the April 18-20, 1967, Spring Joint Computer Conference*, ser. AFIPS '67 (Spring), Atlantic City, New Jersey: Association for Computing Machinery, 1967, pp. 483–485, ISBN: 9781450378956. DOI: 10.1145/1465482.1465560. [Online]. Available: https://doi.org/10.1145/1465482.1465560.

[48] J. L. Gustafson, "Reevaluating amdahl's law," *Commun. ACM*, vol. 31, no. 5, pp. 532–533, May 1988, ISSN: 0001-0782. DOI: 10.1145/42411.42415. [Online]. Available: https://doi.org/10.1145/42411.42415.

[49] EPCC, *Archer2 cu calculator*, 2024. [Online]. Available: https://www.archer2.ac.uk/support-access/cu-calc.html.

[50] J. Jiménez and P. Moin, "The minimal flow unit in near-wall turbulence," *Journal of Fluid Mechanics*, vol. 225, pp. 213–240, 1991. DOI: 10.1017/S0022112091002033.

[51] S. B. Pope, *Turbulent Flows*. Cambridge University Press, 2000.

[52] C. D. Daniel, S. Laizet, and J. C. Vassilicos, "Wall shear stress fluctuations: Mixed scaling and their effects on velocity fluctuations in a turbulent boundary layer," 2017.

[53] NASA Glenn Research Center, *Reynolds number*, 2024. [Online]. Available: https://www.grc.nasa.gov/www/k-12/airplane/reynolds.html.

[54] M. Lee and R. D. Moser, "Direct numerical simulation of turbulent channel flow up to," *Journal of Fluid Mechanics*, vol. 774, pp. 395–415, Jul. 2015, ISSN: 0022-1120. DOI: 10.1017/jfm.2015.268.

[55] L. Könözsy, *Numerical Methods for Incompressible Flows [Course Notes]*, Canvas Cranfield, 2024.

[56] S. Laizet, *XCompact3d Introduction [Course Slide]*, Xcompact3d Course, 2024.

[57] D. G. Westra and J. C. Heinrich, *The fractional step method applied to simulations of natural convective flows*, 2002.

[58] J. van Kan, "A second-order accurate pressure-correction scheme for viscous incompressible flow," *SIAM Journal on Scientific and Statistical Computing*, vol. 7, no. 3, pp. 870–891, 1986. DOI: 10.1137/0907059. eprint: https://doi.org/10.1137/0907059. [Online]. Available: https://doi.org/10.1137/0907059.

[59] N. Li and S. Laizet, "2decompfft - a highly scalable 2d decomposition library and fft interface," in *Cray User Group*, 2010, pp. 1–13.

[60] H. K. Hawez, R. Sanaee, and N. H. Faisal, "A critical review on coupled geomechanics and fluid flow in naturally fractured reservoirs," *Journal of Natural Gas Science and Engineering*, vol. 95, p. 104 150, 2021, ISSN: 1875-5100. DOI: https://doi.org/10.1016/j.jngse.2021.104150. [Online]. Available: https://www.sciencedirect.com/science/article/pii/S1875510021003516.

[61] S. Laizet, *INCOMPACT 3D USER GUIDE version2.0 [User Guide]*, 2024. [Online]. Available: https://www.incompact3d.com/uploads/5/8/7/2/58724623/_user_guide_incompact3d_v2.pdf.

[62] D. R. Durran, "The third-order adams-bashforth method: An attractive alternative to leapfrog time differencing," *Monthly Weather Review*, vol. 119, pp. 702–720, 3 1991.

[63] G. H. Yeoh and J. Tu, "Solution methods for multi-phase flows," in Elsevier, 2010, pp. 95–242. DOI: 10.1016/B978-0-08-046733-7.00003-5.

[64] Ansys, *ANSYS Fluent Mosaic Technology Automatically Combines Disparate Meshes with Polyhedral Elements for Fast, Accurate Flow Resolution [White Paper]*, 2020.

[65] J. Tu, G.-H. Yeoh, and C. Liu, "Chapter 4 - cfd mesh generation: A practical guideline," in *Computational Fluid Dynamics (Third Edition)*, J. Tu, G.-H. Yeoh, and C. Liu, Eds., Third Edition, Butterworth-Heinemann, 2018, pp. 125–154, ISBN: 978-0-08-101127-0. DOI: https://doi.org/10.1016/B978-0-08-101127-

0.00004-0. [Online]. Available: https://www.sciencedirect.com/science/article/pii/B9780081011270000040.

[66] A. Cain, J. Ferziger, and W. Reynolds, "Discrete orthogonal function expansions for non-uniform grids using the fast fourier transform," *Journal of Computational Physics*, vol. 56, pp. 272–286, 2 Nov. 1984, ISSN: 00219991. DOI: 10.1016/0021-9991(84)90096-2.

[67] E. J. Avital, N. D. Sandham, and K. H. Luo, "Stretched cartesian grids for solution of the incompressible navier-stokes equations," *International Journal for Numerical Methods in Fluids*, vol. 33, pp. 897–918, 6 Jul. 2000, ISSN: 02712091. DOI: 10.1002/1097-0363(20000730)33:6<897::AID-FLD37>3.0.CO;2-4.

[68] NASA Glenn Research Center, *Examining spatial (grid) convergence*, 2024. [Online]. Available: https://www.grc.nasa.gov/www/wind/valid/tutorial/spatconv.html.

[69] D. Zhou and K. S. Ball, "Turbulent drag reduction by spanwise wall oscillations," *International journal of engineering. Transactions A: basics*, vol. 21, pp. 85–104, 2008. [Online]. Available: https://api.semanticscholar.org/CorpusID:17940071.

[70] A. Rodriguez-Sevillano, M. Á. Barcala-Montejano, R. Bardera-Mora, and J. Batuecas-Fuejo, "Flow study over bluff bodies based on visualization technique," *American Journal of Science and Technology*, vol. 4, pp. 97–104, 6 2017.

[71] Á. A. Rodríguez-Sevillano, M. J. Casati-Calzada, R. Bardera-Mora, A. Feliz-Huidobro, C. Calle-González, and J. Fernández-Antón, "Flow study on the anemometers of the perseverance based on towing tank visualization," *Applied Mechanics*, vol. 3, no. 4, pp. 1385–1398, 2022, ISSN: 2673-3161. DOI: 10.3390/applmech3040079. [Online]. Available: https://www.mdpi.com/2673-3161/3/4/79.

[72] R. Mittal and S. Balachandar, "On the inclusion of three-dimensional effects in simulations of two-dimensional bluff-body wake flows," in *The 1997 ASME Fluids Engineering Division Summer Meeting*, 1997.

[73] M. Lee and R. D. Moser, "Direct numerical simulation of turbulent channel flow up to $Re_\tau \approx 5200$," *Journal of Fluid Mechanics*, vol. 774, pp. 395–415, 2015. DOI: 10.1017/jfm.2015.268.

[74] T. Munk, D. Kane, and D. Yebra, "The effects of corrosion and fouling on the performance of ocean-going vessels: A naval architectural perspective," in *Ad-*

vances in Marine Antifouling Coatings and Technologies, ser. Woodhead Publishing Series in Metals and Surface Engineering, C. Hellio and D. Yebra, Eds., Woodhead Publishing, 2009, pp. 148–176, ISBN: 978-1-84569-386-2. DOI: https://doi.org/10.1533/9781845696313.1.148. [Online]. Available: https://www.sciencedirect.com/science/article/pii/B9781845693862500077.

[75] J. Southard, "Structure of turbulent boundary layers," in MIT OpenCourseWare, 2024.

[76] I. Marusic, J. P. Monty, M. Hultmark, and A. J. Smits, "On the logarithmic region in wall turbulence," *Journal of Fluid Mechanics*, vol. 716, R3, Feb. 2013, ISSN: 0022-1120. DOI: 10.1017/jfm.2012.511.

[77] R. MATHIS, N. HUTCHINS, and I. MARUSIC, "Large-scale amplitude modulation of the small-scale structures in turbulent boundary layers," *Journal of Fluid Mechanics*, vol. 628, pp. 311–337, 2009. DOI: 10.1017/S0022112009006946.

[78] H. Choi, P. Moin, and J. Kim, "Direct numerical simulation of turbulent flow over riblets," *Journal of Fluid Mechanics*, vol. 255, pp. 503–539, 1993. DOI: 10.1017/S0022112093002575.

[79] L. Agostini, E. Touber, and M. A. Leschziner, "Spanwise oscillatory wall motion in channel flow: Drag-reduction mechanisms inferred from dns-predicted phase-wise property variations at $Re_\tau = 1000$," *Journal of Fluid Mechanics*, vol. 743, pp. 606–635, 2014. DOI: 10.1017/jfm.2014.40.

[80] C.-X. Xu and W.-X. Huang, "Transient response of Reynolds stress transport to spanwise wall oscillation in a turbulent channel flow," *Physics of Fluids*, vol. 17, no. 1, pp. 018101-018101–4, Nov. 2004, ISSN: 1070-6631. DOI: 10.1063/1.1827274. eprint: https://pubs.aip.org/aip/pof/article-pdf/17/1/018101/14692654/018101_1_online.pdf. [Online]. Available: https://doi.org/10.1063/1.1827274.

[81] M. Umair, S. Tardu, and O. Doche, "Reynolds stresses transport in a turbulent channel flow subjected to streamwise traveling waves," *Phys. Rev. Fluids*, vol. 7, p. 054 601, 5 May 2022. DOI: 10.1103/PhysRevFluids.7.054601. [Online]. Available: https://link.aps.org/doi/10.1103/PhysRevFluids.7.054601.

APPENDIX

A Software Choice

Software	Advantages	Disadvantages
Incompact3d	DNS is default	Code structure is harder to read, harder interface
	Written in Fortran, less time to familiarise	Hard to find the documentation, contact must be done through Prof. Laizet
	Collaboration with Ricardo	
OpenFOAM	Code structure is easier to read, better interface	Written in C++, requires additional familiarisation time
	Documentation and guidance is already provided by Tom, easier contact if confused	DNS is harder to set up (requires dnsFoam), a lot of files to set up
		No collaboration?

B CURES

Dear Wahyu

Reference: CURES/23464/2024
Project ID: 25467
Title: Towards the Application of Generalised Richardson Extrapolation in Spanwise Oscillating Wall Flow Control Analysis

Thank you for your application to the Cranfield University Research Ethics System (CURES).

Your proposed research activity has been confirmed as Level 1 risk in terms of research ethics. Your letter of approval will be sent by email within 24 hours. If you do not receive this, please contact CURES Support.

Please remember that CURES occasionally conducts audits of projects. We may therefore contact you during or following execution of your fieldwork. Guidance on good practice is available on the research ethics intranet pages.

If you have any queries, please contact cures-support@cranfield.ac.uk

We wish you every success with your project.

Regards

CURES Team

C ARCHER2 Usage Report

The ARCHER2 resource used is shown in the next page.

SAFE User Usage Report: Wahyu WWD Dyatmika, (wdyatmika)

A total of 40 jobs were submitted by Wahyu WWD Dyatmika, account wdyatmika, during the period Jul - Aug 2024.

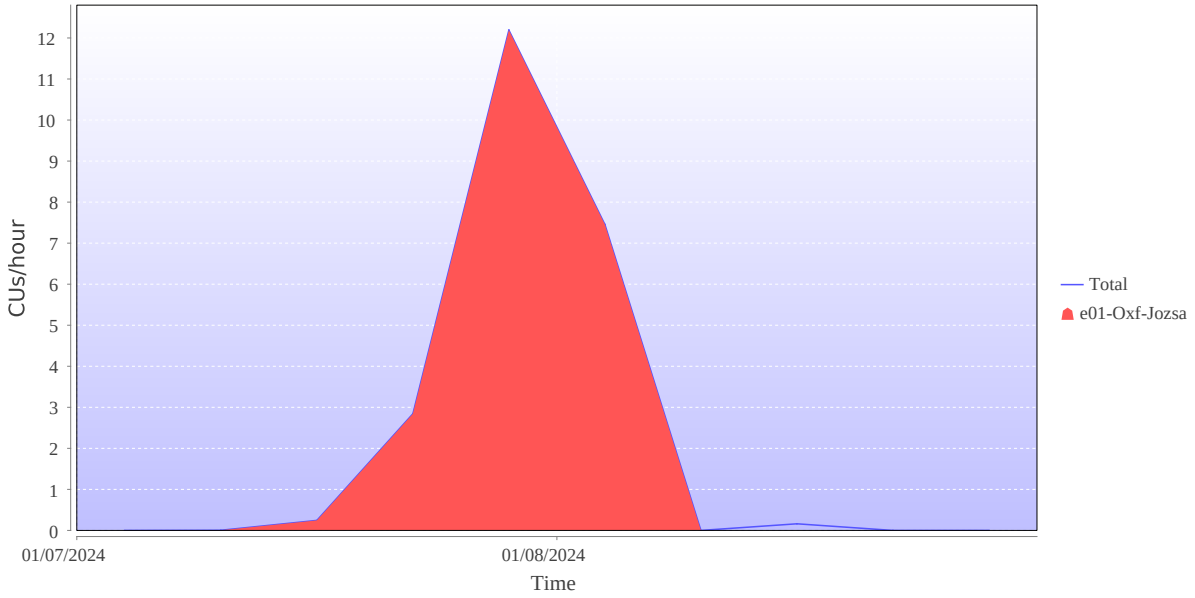

Usage from Archer2

Resource	Budget	Jobs	Charged Usage / CUs	Raw Usage / CUs
Archer2	e01-Oxf-Jozsa	40	3,382.629	3,406.914

Usage broken down by job size.

CPUs	Jobs	Charged Usage / CUs	Raw Usage / CUs
129-256	3	9.005	33.006
257-512	9	25.509	25.794
513-1024	16	33.163	33.163
1025-2048	3	0	0
2049-4096	7	3,314.951	3,314.951
4097-8192	1	0	0
16385-32768	1	0	0

User Jobs Report: Wahyu WWD Dyatmika , account wdyatmika

A total of 37 jobs were submitted by wdyatmika during the period Jul 2024.
Job list for specified period (limited to 100 entries).

Job ID	Job Name	Resourc	Project	Budget	Submit	Start	End	Runtime h	Scheduling Coefficien	Job Size / Nodes	Charged Usage / CUs	Raw Usage / CUs	Job Size / Tasks
7023624	compact3d	Archer2	e01 - UK Turbulence Consortium	e01-Oxf Jozsa	2024-07-12 15:26:56	2024-07-12 15:27:00	2024-07-12 15:44:50	0:17:50	0.996	2	0.594	0.594	0
7062959	compact3d	Archer2	e01 - UK Turbulence Consortium	e01-Oxf Jozsa	2024-07-15 18:15:37	2024-07-15 18:15:43	2024-07-15 18:16:04	0:00:21	0.778	2	0.012	0.012	0
7062968	compact3d	Archer2	e01 - UK Turbulence Consortium	e01-Oxf Jozsa	2024-07-15 18:16:46	2024-07-15 18:16:46	2024-07-15 18:17:03	0:00:17	1	2	0.009	0.009	0
7063343	compact3d	Archer2	e01 - UK Turbulence Consortium	e01-Oxf Jozsa	2024-07-15 19:43:19	2024-07-15 19:54:13	2024-07-15 19:54:23	0:00:10	0.015	2	0.006	0.006	0
7063432	compact3d	Archer2	e01 - UK Turbulence Consortium	e01-Oxf Jozsa	2024-07-15 20:03:58	2024-07-15 20:04:50	2024-07-15 20:05:01	0:00:11	0.175	1	0.003	0.003	0
7072420	compact3d	Archer2	e01 - UK Turbulence Consortium	e01-Oxf Jozsa	2024-07-16 19:07:22	2024-07-16 20:47:44	2024-07-16 20:47:54	0:00:10	0.002	2	0.006	0.006	0
7072827	compact3d	Archer2	e01 - UK Turbulence Consortium	e01-Oxf Jozsa	2024-07-16 22:14:18	2024-07-16 22:17:01	2024-07-16 22:19:09	0:02:08	0.44	2	0.071	0.071	0
7073059	compact3d	Archer2	e01 - UK Turbulence Consortium	e01-Oxf Jozsa	2024-07-16 23:32:10	2024-07-17 01:47:40	2024-07-17 06:47:57	5:00:17	0.689	2	10.009	10.009	0
7080213	compact3d	Archer2	e01 - UK Turbulence Consortium	e01-Oxf Jozsa	2024-07-17 21:48:39	2024-07-18 03:36:37	2024-07-18 12:36:44	9:00:07	0.608	1	9.002	9.002	0
7085489	compact3d	Archer2	e01 - UK Turbulence Consortium	e01-Oxf Jozsa	2024-07-18 13:45:14	2024-07-18 13:49:26	2024-07-18 21:13:30	7:24:04	0.991	2	14.802	14.802	0
7091002	compact3d	Archer2	e01 - UK Turbulence Consortium	e01-Oxf Jozsa	2024-07-19 00:29:43	2024-07-19 00:29:44	2024-07-19 00:29:57	0:00:13	0.929	3	0.011	0.011	0
7091026	compact3d	Archer2	e01 - UK Turbulence Consortium	e01-Oxf Jozsa	2024-07-19 00:32:50	2024-07-19 00:32:54	2024-07-19 01:20:45	0:47:51	0.999	3	2.392	2.392	0
7141294	compact3d	Archer2	e01 - UK Turbulence Consortium	e01-Oxf Jozsa	2024-07-23 15:28:30	2024-07-23 15:28:30	2024-07-23 15:28:30	0:00:00	0	0	0	0	0
7141309	compact3d	Archer2	e01 - UK Turbulence Consortium	e01-Oxf Jozsa	2024-07-23 15:28:46	2024-07-23 15:28:46	2024-07-23 15:28:46	0:00:00	0	0	0	0	0
7141311	compact3d	Archer2	e01 - UK Turbulence Consortium	e01-Oxf Jozsa	2024-07-23 15:28:54	2024-07-23 15:54:18	2024-07-23 15:55:21	0:01:03	0.04	4	0.07	0.07	0
7142416	compact3d	Archer2	e01 - UK Turbulence Consortium	e01-Oxf Jozsa	2024-07-23 18:21:15	2024-07-23 18:21:23	2024-07-23 18:22:14	0:00:51	0.864	4	0.057	0.057	0
7142430	compact3d	Archer2	e01 - UK Turbulence Consortium	e01-Oxf Jozsa	2024-07-23 18:23:05	2024-07-23 18:23:36	2024-07-23 18:24:13	0:00:37	0.544	4	0.041	0.041	0
7142471	compact3d	Archer2	e01 - UK Turbulence Consortium	e01-Oxf Jozsa	2024-07-23 18:28:17	2024-07-23 18:28:48	2024-07-23 18:29:07	0:00:19	0.38	4	0.021	0.021	0
7142481	compact3d	Archer2	e01 - UK Turbulence Consortium	e01-Oxf Jozsa	2024-07-23 18:31:02	2024-07-23 18:31:23	2024-07-23 18:31:41	0:00:18	0.462	4	0.02	0.02	0

Job ID	Job Name	Resourc	Project	Budget	Submit	Start	End	Runtime h	Scheduli Coefficie	Job Size / Nodes	Charged Usage / CUs	Raw Usage / CUs	Job Size / Tasks
7142484	compact3d	Archer2	e01 - UK Turbulence Consortium	e01-Oxf Jozsa	2024-07-23 18:32:38	2024-07-23 18:32:55	2024-07-23 18:35:36	0:02:41	0.904	4	0.179	0.179	0
7142503	compact3d	Archer2	e01 - UK Turbulence Consortium	e01-Oxf Jozsa	2024-07-23 18:36:07	2024-07-23 18:36:38	2024-07-23 18:36:55	0:00:17	0.354	4	0.019	0.019	0
7142511	compact3d	Archer2	e01 - UK Turbulence Consortium	e01-Oxf Jozsa	2024-07-23 18:38:07	2024-07-23 18:38:16	2024-07-23 18:40:07	0:01:51	0.925	4	0.123	0.123	0
7142512	compact3d	Archer2	e01 - UK Turbulence Consortium	e01-Oxf Jozsa	2024-07-23 18:38:09	2024-07-23 18:38:16	2024-07-23 18:38:19	0:00:03	0.3	4	0.003	0.003	0
7142542	compact3d	Archer2	e01 - UK Turbulence Consortium	e01-Oxf Jozsa	2024-07-23 18:42:18	2024-07-23 18:42:32	2024-07-23 18:42:45	0:00:13	0.481	4	0.014	0.014	0
7142547	compact3d	Archer2	e01 - UK Turbulence Consortium	e01-Oxf Jozsa	2024-07-23 18:43:07	2024-07-23 18:43:07	2024-07-23 18:43:07	0:00:00	0	0	0	0	0
7142549	compact3d	Archer2	e01 - UK Turbulence Consortium	e01-Oxf Jozsa	2024-07-23 18:43:18	2024-07-23 18:43:18	2024-07-23 18:43:18	0:00:00	0	0	0	0	0
7142551	compact3d	Archer2	e01 - UK Turbulence Consortium	e01-Oxf Jozsa	2024-07-23 18:43:51	2024-07-23 18:43:51	2024-07-23 18:43:51	0:00:00	0	0	0	0	0
7142552	compact3d	Archer2	e01 - UK Turbulence Consortium	e01-Oxf Jozsa	2024-07-23 18:44:06	2024-07-23 18:44:06	2024-07-23 18:44:06	0:00:00	0	0	0	0	0
7142553	compact3d	Archer2	e01 - UK Turbulence Consortium	e01-Oxf Jozsa	2024-07-23 18:44:17	2024-07-23 18:44:38	2024-07-23 18:46:40	0:02:02	0.853	16	0.542	0.542	0
7142681	compact3d	Archer2	e01 - UK Turbulence Consortium	e01-Oxf Jozsa	2024-07-23 18:47:38	2024-07-23 18:52:34	2024-07-23 18:52:51	0:00:17	0.054	16	0.076	0.076	0
7142717	compact3d	Archer2	e01 - UK Turbulence Consortium	e01-Oxf Jozsa	2024-07-23 18:54:08	2024-07-23 18:56:21	2024-07-23 19:24:12	0:27:51	0.926	16	7.427	7.427	0
7142901	compact3d	Archer2	e01 - UK Turbulence Consortium	e01-Oxf Jozsa	2024-07-23 19:24:41	2024-07-23 19:25:35	2024-07-24 19:25:37	24:00:02	0.999	16	384.009	384.009	0
7155356	compact3d	Archer2	e01 - UK Turbulence Consortium	e01-Oxf Jozsa	2024-07-25 08:47:34	2024-07-25 08:47:44	2024-07-25 08:47:51	0:00:07	0.412	4	0.008	0.008	0
7155363	compact3d	Archer2	e01 - UK Turbulence Consortium	e01-Oxf Jozsa	2024-07-25 08:48:27	2024-07-25 08:49:09	2024-07-25 08:49:18	0:00:09	0.176	4	0.01	0.01	0
7155383	compact3d	Archer2	e01 - UK Turbulence Consortium	e01-Oxf Jozsa	2024-07-25 08:52:38	2024-07-25 08:52:43	2024-07-25 16:01:22	7:08:39	1	4	28.577	28.577	0
7157086	compact3d	Archer2	e01 - UK Turbulence Consortium	e01-Oxf Jozsa	2024-07-25 12:31:10	2024-07-25 12:55:14	2024-07-25 13:19:30	0:24:16	0.502	4	1.618	1.618	0
7166062	compact3d	Archer2	e01 - UK Turbulence Consortium	e01-Oxf Jozsa	2024-07-26 14:48:49	2024-07-26 18:37:25	2024-07-30 18:37:31	96:00:06	0.962	16	1,536.027	1,536.027	0